Inorg. Chem. **2005**, *44*, 3669–3683

Synthesis, Structure, and Characterization of New Mononuclear Mn(II) Complexes. Electrochemical Conversion into New Oxo-Bridged Mn_2(III,IV) Complexes. Role of Chloride Ions

Christelle Hureau,[†,‡] Geneviève Blondin,[†] Marie-France Charlot,[†] Christian Philouze,[§] Martine Nierlich,[||] Michèle Césario,[⊥] and Elodie Anxolabéhère-Mallart*,[†]

Laboratoire de Chimie Inorganique, UMR 8613, LCR-CEA No. 33V, Institut de Chimie Moléculaire et des Matériaux d'Orsay, Université Paris-Sud, 91405 Orsay Cedex, LEDSS, Université Joseph Fourier, Bâtiment Chimie Recherches, 301 Rue de la Chimie, DU BP 53, 38041 Grenoble Cedex 9, DRECAM/SCM, CEA Saclay, Bâtiment 125, 91191 Gif-sur-Yvette, and Laboratoire de Cristallochimie, Institut de Chimie des Substances Naturelles, UPR CNRS 2301, F-91198 Gif-sur-Yvette, France

Received February 16, 2005

Two Mn(II) complexes are isolated and X-ray characterized, namely, *cis*-$[(L^2)Mn^{II}(Cl)_2]$ **(1)** and $[(L^3)Mn^{II}Cl(OH_2)](ClO_4)$ (**2**(ClO_4)), where L^2 and L^3 are the well-known tetradentate *N*,*N*′-dimethyl-*N*,*N*′-bis(2-pyridylmethyl)ethane-1,2-diamine and *N*,*N*′-dimethyl-*N*,*N*′-bis(2-pyridylmethyl)propane-1,3-diamine ligands, respectively. The crystal structure reveals that whereas the ligand L^2 is in the *cis*-α conformation in complex **1**, the ligand L^3 is in the more unusual *cis*-β conformation in **2**. EPR spectra are recorded on frozen solutions for both complexes and are characteristic of Mn(II) species. Electrochemical behaviors are investigated on acetonitrile solution for both complexes and show that cation **2** exists as closely related Mn(II) species in equilibrium. For both complexes exhaustive bulk electrolyses of acetonitrile solution are performed at oxidative potential in various experimental conditions. In the presence of 2,6-lutidine and after elimination of chloride ligands, the formation of the di-μ-oxo mixed-valent complexes $[(L^2)Mn^{III}(\mu\text{-}O)_2Mn^{IV}(L^2)]^{3+}$ **(3a)** and $[(L^3)Mn^{III}(\mu\text{-}O)_2Mn^{IV}(L^3)]^{3+}$ **(4)** is confirmed by UV–vis and EPR spectroscopies and cyclic voltammetry. In addition crystals of **4**$(ClO_4)_3$ were isolated, and the X-ray structure reveals the *cis*-α conformation of L^3. In the absence of 2,6-lutidine and without elimination of the exogenous chloride ions, the electrochemical oxidation of **1** leads to the formation of the mononuclear Mn(III) complex, namely, $[(L^2)Mn^{III}(Cl)_2]^+$ **(5)**, as confirmed by UV–vis as well as parallel mode EPR spectroscopy and cyclic voltammetry. In the same conditions, the electrochemical oxidation of complex **2** is more intricate, and a thorough analysis of EPR spectra establishes the formation of the binuclear mono-μ-oxo mixed-valent $[(L^3)ClMn^{III}(\mu\text{-}O)Mn^{IV}Cl(L^3)]^{3+}$ (**6**) complexes. Electrochemical conversion of Mn(II) complexes into mixed-valent Mn_2(III,IV) oxo-bridged complexes in the presence of 2,6-lutidine is discussed. The role of the chloride ligands as well as that of L^3 in the building of oxo bridges is discussed. Differences in behavior between L^2 and L^3 are commented on.

Introduction

Manganese ions are involved in numerous biological redox reactions performed by metalloenzymes.[1] In these natural systems, Mn ions exist in different oxidation states in active sites presenting various nuclearities. A mononuclear center is the active site of superoxide dismutase (Mn−SOD),[2] where superoxide is converted into dioxygen and hydrogen peroxide.[3] Manganese catalases, responsible for the dispropor-

* To whom correspondence should be addressed. E-mail: eanxolab@icmo.u-psud.fr.
[†] Université Paris-Sud.
[‡] Current address: LBSO, Service de Bioénergétique, CNRS URA 2096, Département de Biologie Joliot Curie, CEA Saclay, Bâtiment 532, 91191 Gif-sur-Yvette, France.
[§] Université Joseph Fourier.
[||] CEA Saclay.
[⊥] UPR CNRS 2301.

(1) Larson, E. J.; Pecoraro, V. L. In *Manganese Redox Enzymes*; Pecoraro, V. L., Ed.; VCH Publishers: New York, 1992; pp 1−28.
(2) Yoder, D. W.; Hwang, J.; Penner-Hahn, J. E. In *Metal Ions in Biological processes*; Sigel, A., Sigel, H., Eds.; Marcel-Dekker: Basel, Switzerland, 2000; pp 527−557.
(3) Penner-Hahn, J. E. *Struct. Bonding (Berlin)* **1998**, *90*, 1−36.

10.1021/ic050243y CCC: $30.25
Published on Web 04/12/2005

tionation of hydrogen peroxide into water and dioxygen, possess a dinuclear center which oscillates between Mn(II)-Mn(II) and Mn(III)Mn(III) during the catalytic cycle.[4] The oxygen evolving center (OEC) of photosystem II, where water is split into dioxygen and protons, is one of the most intensively studied catalytic sites, but still remains a mysterious molecular machinery.[5−7] Resolution of the recently published X-ray diffraction studies has improved down to 3.5 Å.[8] The authors proposed that the four Mn ions of the active site are disposed in a "3 + 1" tetranuclear complex. Three of the manganese ions and one calcium ion are at the corners of a distorted cube, with oxygen atoms at the other corners of the cube. Thus, Mn pairs are connected by di-μ-oxo units. The fourth Mn ion is liganded by one unsupported mono-μ-oxo bridge to one Mn ion of the cube. The water splitting reaction requires four oxidizing equivalents, which are photogenerated and stored by the OEC. Kok et al. have shown that the OEC goes through five oxidation states, denoted S_0 to S_4, dioxygen being released in the S_4 to S_0 transition.[9,10] X-ray absorption techniques and EPR spectroscopy have established that the Mn ions are present in the +II, +III, and/or +IV oxidation states.[11−13] Polynuclear Mn−oxo complexes have been studied as models for this active site.[14−30] Indeed, comparison of the spectroscopic signature of the active site with those of structurally well characterized synthetic complexes has been an intensively developed strategy. As an example, in a comparison with di-μ-oxo-bridged dinuclear Mn(III)Mn(IV) complexes, EPR and X-ray absorption spectroscopies evidenced the presence of such a dinuclear unit in the S_2 state.[31] Developing new models remains a challenging task, since it is still an accurate method to investigate the separate S-states of the catalytic cycle. In this context, we have focused our interest on building dinuclear Mn(III)Mn(IV) complexes with either di-μ-oxo or mono-μ-oxo bridges. These two types of complexes could be distinguished by their EPR signatures, as we have evidenced in one of our previous papers.[32] Furthermore, as chloride ion is proposed to play a special role in the OEC function,[33] it is equally of interest to investigate the synthesis of oxo-bridged Mn complexes in the presence of chloride ions.[34]

Whereas the chemical synthesis of such oxo-bridged dinuclear Mn complexes is well documented in the literature, their electrochemical preparation has not been intensively developed. Consequently, it is of great interest to investigate the reasoned formation of oxo-bridged high-valent complexes from low-valent mononuclear metallic ion complexes. The pioneer work in this area was performed by Sawyer using the 2,2′-bipyridine (bpy) and 1,10-phenantroline (phen) bidentate ligands.[35,36] More recently similar work has been deepened with tridentate ligands, namely, 2,2′:6,2"-terpyridine (terpy)[23] and *N*,*N*-bis-(2-pyridylmethyl)ethanamine (bpea).[37−39] The use of a tridentate ligand in place of a bidentate ligand allowed the authors to generate a new kind of oxo-bridged complex. The formation of the oxo bridges is driven by the deprotonation of water molecules. We shall emphasize that, in these cited works, it is either the ligand itself or the acetate ions introduced with the starting Mn(II)

(4) Barynin, V. V.; Whittaker, M. M.; Antonyuk, S. V.; Lamzin, V. S.; Harrison, P. M.; Artymiuk, P. J.; Whittaker, J. W. *Structure* **2001**, *9*, 725−738.
(5) Yachandra, V. K. *Philos. Trans. R. Soc. London, B* **2002**, *357*, 1347−1358.
(6) Rutherford, A. W.; Faller, P. *Trends Biochem. Sci.* **2001**, *26*, 341−344.
(7) Rutherford, A. W.; Boussac, A. *Science* **2004**, *303*, 1782−1784.
(8) Ferreira, K. N.; Iverson, T. M.; Maghlaoui, K.; Barber, J.; Iwata, S. *Science* **2004**, *303*, 1831−1838.
(9) Joliot, P.; Barbieri, G.; Chabaud, R. *Photochem. Photobiol.* **1969**, *10*, 309−329.
(10) Kok, B.; Forbush, B.; McGloin, M. *Photochem. Photobiol.* **1970**, *11*, 457−475.
(11) Sauer, K.; Yachandra, V. K.; Britt, R. D.; Klein, M. P. In *Manganese Redox Enzymes*; Pecoraro, V. L., Ed.; VCH: New York, 1992; pp 141−175.
(12) Carrell, T. G.; Tyryshkin, A. M.; Dismukes, G. C. *J. Biol. Inorg. Chem.* **2002**, *7*, 2−22.
(13) Bergmann, U.; Grush, M. M.; Horne, C. R.; DeMarois, P.; Penner-Hahn, J. E.; Yocum, C. F.; Wright, D. W.; Dube, C. E.; Armstrong, W. H.; Christou, G. *J. Phys. Chem. B* **1998**, *102*, 8350−8352.
(14) Mukhopadhyay, S.; Mandal, S. K.; Bhaduri, S.; Armstrong, W. H. *Chem. Rev.* **2004**, *104*, 3981−4026.
(15) Pecoraro, V. L.; Hsieh, W.-Y. In *Metals in Biological Systems*; Sigel, A., Sigel, H., Eds.; Marcel-Dekker: Basel, Switzerland, 2000; Vol. 37, pp 429−504.
(16) Glerup, J.; Goodson, P. A.; Hazell, A.; Hazell, R.; Hodgson, D. J.; McKenzie, C. J.; Michelsen, K.; Rychlewska, U.; Toftlund, H. *Inorg. Chem.* **1994**, *33*, 4105−4111.
(17) Philouze, C.; Blondin, G.; Girerd, J.-J.; Guilhem, J.; Pascard, C.; Lexa, D. *J. Am. Chem. Soc.* **1994**, *116*, 8557−8565.
(18) Gelasco, A.; Kirk, M. L.; Kampf, J. W.; Pecoraro, V. L. *Inorg. Chem.* **1997**, *36*, 1829−1837.
(19) Pal, S.; Armstrong, W. H. *Inorg. Chem.* **1992**, *31*, 5417−5423.
(20) Horner, O.; Anxolabéhère-Mallart, E.; Charlot, M.-F.; Tchertanov, L.; Guilhem, J.; Mattioli, T. A.; Boussac, A.; Girerd, J.-J. *Inorg. Chem.* **1999**, *38*, 1222−1232.
(21) Horner, O.; Charlot, M.-F.; Boussac, A.; Anxolabéhère-Mallart, E.; Tchertanov, L.; Guilhem, J.; Girerd, J.-J. *Eur. J. Inorg. Chem.* **1998**, 721−727.
(22) Frapart, Y.-M.; Boussac, A.; Albach, R.; Anxolabéhère-Mallart, E.; Delroisse, M.; Verlach, J.-B.; Blondin, G.; Girerd, J.-J.; Guilhem, J.; Cesario, M.; Rutherford, A. W.; Lexa, D. *J. Am. Chem. Soc.* **1996**, *118*, 2669−2678.
(23) Baffert, C.; Collomb, M.-N.; Deronzier, A.; Pécaut, J.; Limburg, J.; Crabtree, R. H.; Brudvig, G. W. *Inorg. Chem.* **2002**, *41*, 1404−1411.
(24) Ruettinger, W. F.; Ho, D. N.; Dismukes, G. C. *Inorg. Chem.* **1999**, *38*, 1036−1037.
(25) Mukhopadhyay, S.; Staples, R. J.; Armstrong, W. H. *Chem. Commun.* **2002**, 864−865.
(26) Ruettinger, W. F.; Campana, C.; Dismukes, G. C. *J. Am. Chem. Soc.* **1997**, *119*, 6670−6671.
(27) Dube, C. E.; Sessoli, R.; Hendrich, M. P.; Gatteschi, D.; Armstrong, W. H. *J. Am. Chem. Soc.* **1999**, *121*, 3537−3538.
(28) Hsieh, W.-Y.; Campbell, K. A.; Gregor, W.; Britt, R. D.; Yoder, D. W.; Penner-Hahn, J. E.; Pecoraro, V. L. *Biochim. Biophys. Acta* **2004**, *1655*, 149−157.
(29) Ashmawy, F. M.; McAuliffe, C. A.; Parish, R. V.; Tames, J. *J. Chem. Soc., Dalton Trans.* **1985**, 1391−1397.
(30) Aurangzeb, N.; Hulme, C. E.; McAuliffe, C. A.; Pritchard, R. G.; Watkinson, M.; Bermejo, M. R.; Garcia-Deibe, A.; Rey, M.; Sanmartin, J.; Sousa, A. *J. Chem. Soc., Chem. Commun.* **1994**, 1153−1155.
(31) Yachandra, V. K.; Sauer, K.; Klein, M. P. *Chem. Rev.* **1996**, *96*, 2927−2950.
(32) Hureau, C.; Sabater, L.; Anxolabéhère-Mallart, E.; Nierlich, M.; Charlot, M.-F.; Gonnet, F.; Rivière, E.; Blondin, G. *Chem.—Eur. J.* **2004**, *10*, 1998−2010.
(33) Homann, P. H. *Photosynth. Res.* **2002**, *73*, 169−175.
(34) Triller, M. U.; Hsieh, W.-Y.; Pecoraro, V. L.; Rompel, A.; Krebs, B. *Inorg. Chem.* **2002**, *41*, 5544−5554.
(35) Morrison, M. M.; Sawyer, D. T. *J. Am. Chem. Soc.* **1977**, *99*, 257−258.
(36) Morrison, M. M.; Sawyer, D. T. *Inorg. Chem.* **1978**, *17*, 333−337.
(37) Collomb Dunand-Sauthier, M.-N.; Deronzier, A.; Romero, I. *J. Electroanal. Chem.* **1997**, *436*, 219−225.
(38) Mahapatra, S.; Lal, T. K.; Mukherjee, R. *Inorg. Chem.* **1994**, *33*, 1579−1580.
(39) Romero, I.; Dubois, L.; Collomb, M.-N.; Deronzier, A.; Latour, J.-M.; Pécaut, J. *Inorg. Chem.* **2002**, *41*, 1795−1806.

Chart 1

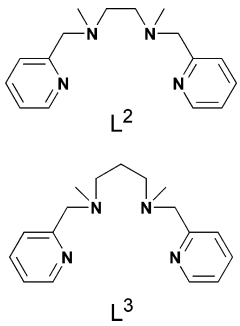

compound which are in charge of the deprotonation process. In one of our previous works,[40] we reported the controlled electrochemical conversion of a heptacoordinated Mn(II) complex into various di-μ-oxo-di-Mn core complexes. The addition of an external base, namely, the 2,6-dimethylpyridine named 2,6-lutidine, allowed the role of the ligand in the deprotonation of water molecules to be tackled. In another work, we also reported the use of 2,6-lutidine in the electrochemical formation of a mono-μ-oxo dinuclear Mn_2(III,IV) complex from a dinuclear Mn_2(II,II) complex.[32] In this work, we will show that this method can indeed be enlarged.

We report here the synthesis and crystal structure of two new mononuclear Mn(II) complexes, *cis*-$[(L^2)Mn^{II}Cl_2]$ (**1**) and $[(L^3)Mn^{II}Cl(OH_2)](ClO_4)$ (**2**(ClO_4)), where L^2 and L^3 are, respectively, the tetradentate ligands *N*,*N*′-dimethyl-*N*,*N*′-bis-(2-pyridylmethyl)ethane-1,2-diamine and *N*,*N*′-dimethyl-*N*,*N*′-bis(2-pyridylmethyl)propane-1,3-diamine (see Chart 1). Frozen-solution X-band EPR spectroscopy of **1** and **2** has been investigated. Cyclic voltammetry reveals that complexes **1** and **2** have different behaviors in acetonitrile solution.

We will demonstrate that, in the presence of base, namely, the 2,6-dimethylpyridine, and in the absence of chloride ions, electrochemical oxidation of **1 (**respectively **2)** leads to the formation of the di-μ-oxo-bridged dinuclear cations $[(L^2)Mn^{III}(\mu\text{-}O)_2Mn^{IV}(L^2)]^{3+}$ (**3a**) **(**respectively $[(L^3)Mn^{III}(\mu\text{-}O)_2Mn^{IV}(L^3)]^{3+}$ (**4**)). Remarkably, compound **4** has never been obtained using a conventional chemical method, in contrast with complex **3a** and similar numerous related complexes.[16,21,22,41−44] The X-ray structure of the new compound **4**$(ClO_4)_3$ is reported. Keeping in mind that the presence of an anionic ligand in the Mn coordination sphere should sustain the formation of unsupported mono-μ-oxo-bridged dinuclear complexes,[20,32,34,45] we also investigated the electrochemical oxidation of **1** and **2** in the presence of chloride ions. The electrochemical preparations of the monomeric $[(L^2)Mn^{III}(Cl)_2]^+$ cation (**5**) and of the unsupported mono-μ-oxo $[(L^3)ClMn^{III}(\mu\text{-}O)Mn^{IV}Cl(L^3)]^{3+}$ complex (**6**) are reported. The present work illustrates how the use of an external base and/or exogenous anionic ligand allows the building of various bridges.

Experimental Section

General Remarks. Reagents and solvents were purchased commercially and used as received except for electrochemical experiments for which acetonitrile was distilled under argon over granular $CaCl_2$.

Caution: *Perchlorate salts of metal complexes with organic ligands are potentially explosive. Only small quantities of these compounds should be prepared and handled behind suitable protective shields!*

Syntheses. The syntheses of ligands L^2 and L^3 have been reinvestigated, and the following route has been used: 0.1 mol of ethane-1,2-diamine (respectively propane-1,3-diamine) and 0.2 mol of 2-pyridinecarboxaldehyde are mixed in 100 mL of methanol and heated to 80 °C for 2 h. After cooling, the imine functions thus obtained are reduced by addition of 0.25 mol of sodium borohydride. During the addition, the solution is maintained at 0 °C. After the addition, the solution is heated to 100 °C for 1 h. Then, chlorhydric acid (5 M) is added to reach pH 4. After addition of sodium hydroxide to pH 9, the white precipitate that appears is filtered out. Methanol is eliminated, and the residual aqueous solution is extracted three times with 50 mL of chloroform. Methylation of the amine functions is obtained by adding 3 mL of water, 22 mL of formic acid, and 18 mL of formaldehyde to 40 mmol of the previous ligand. The mixture is heated to 85 °C for 3 days. After cooling, sodium hydroxide (7.5 M) is added to obtain pH > 12. The aqueous solution is extracted three times with 50 mL of chloroform. L^2 and L^3 are yellow oils, obtained, respectively, with 72% and 73% yields. ^{1}H NMR (200 MHz, $CDCl_3$): δ (L^2) 2.25 (s, 3H), 2.65 (s, 2H), 3.15 (s, 2H), 7.4 (m, 3H), 8.45 (d, H); (L^3) 1.70 (quint, H), 2.20 (s, 3H), 2.50 (s, 2H), 3.60 (s, 2H), 7.5 (m, 3H), 8.45 (d, H).

***cis*-$[(L^2)Mn(Cl)_2]\cdot 0.5H_2O$ (1·0.5H_2O).** To a 3 mL acidic aqueous solution (0.1 M HCl, pH 1) of 2.0 mmol of L^2 was added 2.0 mmol of $MnCl_2\cdot 4H_2O$. The solution is stirred for 15 min, and the white precipitate thus obtained is filtrated on a frit and washed carefully with ethanol (yield 67%). Crystals of **1** suitable for X-ray crystallography are obtained by slow diffusion of ether in an acetonitrile solution of **1**. Anal. Calcd for $C_{16}H_{23}N_4O_{0.5}MnCl_2$: C, 47.37; H, 5.84; N, 13.81; Cl, 17.90. Found: C, 47.5; H, 5.8; N, 13.8; Cl, 17.5. IR: ν (cm^{-1}) = 3493 (S, strong), 3433 (S), 2973 (w; weak), 2879 (w), 1626 (w), 1601 (S), 1570 (m, medium), 1478 (m), 1465 (m), 1432 (S), 1372 (m), 1304 (S), 1268 (m), 1192 (m), 1162 (w), 1140 (w), 1082 (S), 1053 (S), 1028 (S), 1014 (S), 977 (S), 950 (w), 917 (w), 816 (S), 779 (S), 730 (m), 639 (m), 591 (w), 539 (m). ESI MS: The major peak is detected at m/z = 360 and corresponds to $[(L^2)MnCl]^+$.

$[(L^3)MnCl(OH_2)](ClO_4)\cdot H_2O$ (2$(ClO_4)\cdot H_2O$). To a 3 mL acidic aqueous solution (0.1 M HCl, pH 1) of 2.0 mmol of L^3 was added 2.0 mmol of $MnCl_2\cdot 4H_2O$. The solution is stirred for 15 min and 4.0 mmol of sodium perchlorate added. Crystals of **2** suitable for X-ray crystallography are obtained by slow evaporation of the solution (yield 72%). Anal. Calcd for $C_{17}H_{28}N_4O_6MnCl_2$: C, 40.02; H, 5.53; N, 10.98; Cl, 13.90. Found: C, 40.0; H, 5.6; N, 10.7; Cl, 13.5. IR: ν (cm^{-1}) = 3598 (m), 3362 (m), 2972 (w), 2915 (w), 2828 (w), 2015 (w), 1656 (m), 1602 (S), 1570 (m), 1485 (w), 1470 (m), 1443 (m), 1403 (w), 1363 (w), 1324 (w), 1302 (m), 1264 (w), 1250 (w), 1222 (w), 1206 (w), 1182 (w), 1155 (w), 1108 (S), 1091

(40) Hureau, C.; Blanchard, S.; Nierlich, M.; Blain, G.; Rivière, E.; Girerd, J.-J.; Anxolabéhère-Mallart, E.; Blondin, G. *Inorg. Chem.* **2004**, *43*, 4415−4426.
(41) Goodson, P. A.; Glerup, J.; Hodgson, D. J.; Michelsen, K.; Weihe, H. *Inorg. Chem.* **1991**, *30*, 4909−4914.
(42) Goodson, P. A.; Glerup, J.; Hodgson, D. J.; Michelsen, K.; Pedersen, E. *Inorg. Chem.* **1990**, *29*, 503−508.
(43) Goodson, P. A.; Hodgson, D. J.; Glerup, J.; Michelsen, K.; Weihe, H. *Inorg. Chim. Acta* **1992**, *197*, 141−147.
(44) Goodson, P. A.; Hodgson, D. J. *Inorg. Chem.* **1989**, *28*, 3606−3608.
(45) Baffert, C.; Collomb, M.-N.; Deronzier, A.; Kjærgaard-Knudsen, S.; Latour, J.-M.; Lund, K. H.; McKenzie, C. J.; Mortensen, M.; Preuss Nielsen, L.; Thorup, N. *Dalton Trans.* **2003**, 1765−1772.

Table 1. Details of Structure Determination, Refinement, and Experimental Parameters for Compounds **1**, **2**, and **4**

	1	**2**	**4**
empirical formula	$C_{16}H_{22}Cl_2N_4Mn$	$C_{17}H_{28}Cl_2N_4MnO_6$	$C_{40}H_{57}Cl_3N_{11}Mn_2O_{14}$
fw	396.22	510.28	1132.2
temp (K)	295 (2)	293 (2)	123 (2)
wavelength (Å)	0.71070	0.71073	0.71073
cryst syst	orthorhombic	monoclinic	triniclic
space group	*Pbcn*	*P*21/*c*	$P\bar{1}$
a (Å)	14.425(2)	9.64(1)	12.178(2)
b (Å)	8.1970(10)	17.27(2)	12.446(3)
c (Å)	15.164(4)	13.73(1)	17.641(4)
α (deg)			102.05(3)
β (deg)		97.0(1)	104.62(3)
γ (deg)			98.22(3)
vol (Å^3)	1793.0(6)	2268(4)	2475.5(9)
Z	4	4	2
density(calcd) (g·cm^{-3})	1.468	1.494	1.519
abs coeff (mm^{-1})	1.038	0.857	0.747
cryst size (mm)	0.54 × 0.45 × 0.36	0.24 × 0.18 × 0.10	0.12 × 0.10 × 0.05
θ range for data collection (deg)	2.69−29.97	1.18−29.96	2.47−24.70
index ranges	$-20 \le h \le +20$	$-13 \le h \le +13$	$0 \le h \le +14$
	$0 \le k \le +11$	$0 \le k \le +9$	$-14 \le k \le +14$
	$0 \le l \le +21$	$0 \le l \le +19$	$-20 \le l \le +19$
no. of reflns collected	5126	7055	15132
no. of independent reflns	2616 [*R*(int) = 0.0627]	6945 [*R*(int) = 0.0627]	7721 [*R*(int) = 0.1820]
no. of data	2616	6945	2903
no. of params	106	271	667
goodness-of-fit on F^2	1.112	1.983	0.985
final *R* indices [$I > 2\sigma(I)$]	R1 = 0.0394	R1 = 0.0664	R1 = 0.0912
	wR2 = 0.1089	wR2 = 0.0988	wR2 = 0.1744
R indices (all data)	R1 = 0.601	R1 = 0.1097	R1 = 0.2575
	wR2 = 0.1252	wR2 = 0.1091	wR2 = 0.2405
largest diff peak/hole (e$^-$·Å^{-3})	0.795/−0.531	0.57/−0.52	0.559/−0.491

(S), 1012 (w), 990 (w), 909 (w), 847 (w), 771 (S), 623 (S). ESI MS: One major peak is detected at $m/z = 374$ that corresponds to $[(L^3)MnCl]^+$.

$[(L^3)Mn(\mu\text{-}O)_2Mn(L^3)](ClO_4)_3$ ($4(ClO_4)_3$). Crystals suitable for X-ray crystallography were obtained by cooling to −20 °C the solution resulting from the electrolysis of compound **2**$(ClO_4)\cdot H_2O$. The electrolysis was performed after filtration of silver chloride salt resulting from precipitation of chloride ion by 1 equiv of silver perchlorate and in the presence of 2 equiv of 2,6-lutidine per Mn ion.

Physical Measurements. Elemental analyses were performed by the Service de Microanalyse of the CNRS (Gif sur Yvette, France) for carbon, nitrogen, and hydrogen and by the Service Central d'Analyse of CNRS (Vernaison, France) for chlorine. Infrared spectra were recorded on KBr pellets in the range of 4000−200 cm^{-1} with a Perkin-Elmer Spectrum 1000 spectrophotometer. ^{1}H NMR spectra were recorded using a Bruker AC-200 (200 MHz) or a Bruker AM-250 (250 MHz). Electrospray ionization mass spectra were recorded with a Finnigan Mat Mat95S in BE configuration at low resolution on micromolar acetonitrile solutions.

X-ray Crystallography. Crystallographic data for **1**, **2**, and **4** are given in Table 1.

The *Pbcn* orthorhombic yellow prism (∼0.54 × 0.45 × 0.36 mm^3) of compound **1** was obtained by slow diffusion of ether into an acetonitrile solution of **1**, and the monoclinic brown prism (∼0.24 × 0.18 × 0.10 mm^3) of compound **2**$(ClO_4)\cdot H_2O$ was rapidly formed from an aqueous solution of **2**. Both crystals were stuck on a glass fiber and centered on the goniometer of a Nonius (Bruker) CAD-4 diffractometer. Unit cell parameters were obtained by least-squares refinement with the CAD-4 software[46] of 25 reflections that had been automatically centered on the diffractometer. The crystal decay was 5% for **1** and 14.5% for **2**. Intensity data were collected with the CAD-4 software. Then for **1**, the data were processed and the structure was solved using the SHELX programs.[47,48] For **2**, the data were processed using the TeXsan program package. The structure was solved by direct methods with the use of the SIR92 software[49] and refined using TeXsan. The extinction was refined. The final refinement involved an anisotropic model for all non-hydrogen atoms. The hydrogen atoms were set geometrically or using the difference Fourier. They were recalculated before the last refinement cycle. The model displays two hydrogen bonds for compound **2**.

Crystal data for **4**$(ClO_4)_3$ were collected on a Nonius Kappa-CCD area detector diffractometer[50] using graphite-monochromated Mo Kα radiation. The lattice parameters were determined from 10 images recorded with 2° φ scans and later refined on all data. The data were recorded at 123 K. A 180° φ range was scanned with 2° steps with a crystal to detector distance fixed at 30 mm. Data were corrected for Lorentz polarization. The structures were solved by direct methods with SHELXS-97[51] and refined by full-matrix least-squares on F^2 with anisotropic thermal parameters for all non-H atoms with SHELXL-97.[52] One perchlorate anion (Cl1) was found disordered on two positions with 0.7 and 0.3 occupation factors. H atoms (except H atoms of one solvent molecule, CH_3CN) were introduced at calculated positions as riding atoms with an isotropic displacement parameter equal to 1.2 (CH and CH_2) or 1.5 (CH_3)

(46) Enraf-Nonius CAD-4 Software, 1989.

(47) Sheldrick, G. M. *Acta Crystallogr., Sect. A: Found. Crystallogr.* **1990**, *46*, 467.

(48) Sheldrick, G. M. *SHELXL-93: Program for the refinement of crystal structures*; University of Göttingen: Göttingen, Germany, 1993.

(49) Altomare, A.; Cascarano, G.; Giacovazzo, C.; Guagliardi, A. *J. Appl. Crystallogr.* **1993**, *26*, 343−350.

(50) Nonius B.V. *Kappa-CCD Software*; Nonius B.V.: Delft, The Netherlands, 1998.

(51) Sheldrick, G. M. *Acta Crystallogr., Sect. A: Found. Crystallogr.* **1990**, *46*, 467.

(52) Sheldrick, G. M. *SHELXL-97: Program for the Refinement of Crystal Structures*; University of Göttingen: Göttingen, Germany, 1997.

times that of the parent atom. The molecular plots were drawn with SHELXTL.[53] All calculations were performed on a Silicon Graphics R10000 workstation.

Crystallographic data (excluding structure factors) have been deposited at the Cambridge Crystallographic Data Center as Supplementary Publication Numbers CCDC-233920 (**1**), CCDC-228080 (**2**), and CCDC-226852 (**4**). Copies of the data can be obtained free of charge on application to CCDC, 12 Union Rd., Cambridge CB21EZ, U.K. Fax (+44) 1223-336-033. E-mail: deposit@ccdc.cam.ac.uk.

EPR Spectroscopy. X-band EPR spectra were recorded on a Bruker ELEXSYS 500 spectrometer. For low-temperature studies, an Oxford Instrument continuous flow liquid helium cryostat and a temperature control system were used. Simulations of complexes **3**, **4**, and **6** spectra were performed using a program described in ref 54. An $S = 1/2$ system was considered, and the EPR spectrum profile was assumed to be governed by the Zeeman effect within the $S = 1/2$ state and the two hyperfine interactions between the $S = 1/2$ electronic spin on one hand and the $I = 5/2$ nuclear spin on the other. The following Hamiltonian was used: $\hat{H} = \mu_B B[\mathbf{g}]\hat{S} + \hat{S}[\mathbf{A}_1]\hat{I}_1 + \hat{S}[\mathbf{A}_2]\hat{I}_2$. Only the electronic and nuclear spin values are introduced to perform the EPR simulation, and no hypothesis is formulated on the oxidation states of the manganese ion. A Gaussian line shape was used.

The EPR signal of species **6** was obtained by successive subtractions of the other signals of Mn(II) species and of complex **4** present in the spectrum recorded during the course of the bulk electrolysis. First, the quantity of $[(L^3)Mn^{II}(S)_2]^{2+}$, $[(L^3)Mn^{II}Cl(S)]^{+}$, and $[(L^3)Mn^{II}(Cl)_2]$, depending on the electrolysis performed, is estimated by scaling the transition at low field. Second, the quantity of solvated Mn(II) is estimated by comparison with spectra of varying concentration of pure species of solvated Mn(II). Third, the contribution of complex **4** is estimated by scaling the absorption of the two outermost lines of the signal of species **4**. All these contributions are then subtracted. This general method was applied for the various electrolysis experiments, and all the different signals obtained were highly similar.

The signal used for the simulation presented in this work has been obtained as follows. Contributions from solvated Mn(II) and species **4** were eliminated by obtaining the difference between the spectrum recorded after consumption of 0.6 e^- per Mn ion (Figure 11b) and 43% of the spectrum recorded after consumption of 0.8 e^- per Mn ion (data not shown) during the bulk electrolysis of complex **2**. This was made possible since the amounts of solvated Mn(II) and species **4** during the course of the electrolysis increase identically. An ultimate subtraction of 20% of the initial signal (Figure 11a) allows us to obtain a signature suitable for EPR simulation.

Cyclic Voltammetry and Bulk Electrolyses. Cyclic voltammetry and coulometry measurements were recorded thanks to an EG&G PAR potentiostat (M273 model). For cyclic voltammetry the counter electrode was a Au wire and the working electrode a glassy carbon disk carefully polished before each voltammogram with a 1 μm diamond paste, sonicated in an ethanol bath, and then washed carefully with ethanol. The reference electrode was a $Ag/AgClO_4$ electrode (0.530 V vs NHE electrode), isolated in a fritted bridge. For bulk electrolyses, the counter electrode was a piece of Pt, separated from the rest of the solution with a fritted bridge. The working electrode was a Pt grid of approximately 24 cm^2. The solvent used was distilled acetonitrile, and tetrabutylammonium perchlorate was added to obtain a 0.1 M supporting electrolyte, or 0.2 M when the experiments are carried out at low temperature (below 10 °C). Low-temperature regulation was ensured by a Julabo circulation cryostat. The oxidation potential of free chloride ions in acetonitrile was measured on a 1 mM solution of tetraethylammonium chloride ($(C_2H_5)_4NCl$) at room temperature.

UV−Vis Spectroscopy. UV−vis spectra were recorded on a Varian Cary 300 Bio or a Varian Cary 5E spectrophotometer at 20 °C with either 0.1 or 1 cm quartz cuvettes.

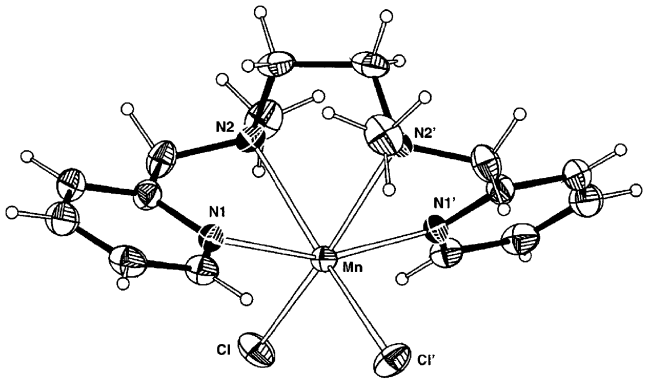

Figure 1. Molecular view of **1**.

Table 2. Selected Bond Lengths (Å) and Angles (deg) for **1**

Mn−Cl	2.4505(7)	Mn−N2	2.366(2)
Mn−N1	2.278(2)		
Cl−Mn−Cl′ [a]	103.83(4)	N1−Mn−N1′	159.38(9)
Cl−Mn−N1	98.52(5)	N1−Mn−N2	71.90(6)
Cl−Mn−N1′	94.17(5)	N1−Mn−N2′	91.67(6)
Cl−Mn−N2	91.47(5)	N2−Mn−N2′	76.27(9)
Cl−Mn−N2′	160.85(5)		

[a] Symmetry transformation used to generate equivalent atoms: $-x + 1$, y, $-z + 3/2$.

Results

The reaction of L^2 with manganese(II) chloride in acidic (0.1 M HCl) solution gives *cis*-$[(L^2)Mn(Cl)_2]$ (**1**). $[(L^3)MnCl(OH_2)]$ (**2**) is obtained after the addition of perchlorate sodium salt to a similar acidic solution prepared with L^3 (see the Experimental Section).

Crystal Structure of *cis*-$[(L^2)Mn(Cl)_2]$ (1). The crystal structure of compound **1** is represented in Figure 1, and principal bond lengths and angles are listed in Table 2. The Mn(II) ion is coordinated by the four nitrogen atoms of the L^2 ligand, and two exogenous chloride anions. The two chloride anions are in *cis* positions and the two pyridine groups of L^2 *trans* to one another. Consequently, the L^2 ligand folds around the metal ion using the *cis*-α conformation usually observed within this family of aminopyridine ligands.[16,41,42,55−57] The complex presents a C_2 axis that bisects the Cl−Mn−Cl′ angle. The Mn(II) is in a distorted octahedral

(53) Sheldrick, G. M. *SHELXTL*, Version 5.1; distributed by Bruker AXS, Madison, WI, University of Göttingen: Göttingen, Germany, 1999.
(54) Blondin, G.; Davydov, R.; Philouze, C.; Charlot, M.-F.; Styring, S.; Akermark, B.; Girerd, J.-J.; Boussac, A. *J. Chem. Soc., Dalton Trans.* **1997**, 4069−4074.
(55) Glerup, J.; Goodson, P. A.; Hodgson, D. J.; Michelsen, K.; Nielsen, K. M.; Weihe, H. *Inorg. Chem.* **1992**, *31*, 4611−4616.
(56) Raffard-Pons y Moll, N.; Balland, V.; Simaan, A. J.; Letard, S.; Nierlich, M.; Miki, K.; Banse, F.; Anxolabéhère-Mallart, E.; Girerd, J.-J. *C. R. Chim. 5* **2002**, 99−109.
(57) Poussereau, S.; Blondin, G.; Cesario, M.; Guilhem, J.; Chottard, G.; Gonnet, F.; Girerd, J.-J. *Inorg. Chem.* **1998**, *37*, 3127−3132.

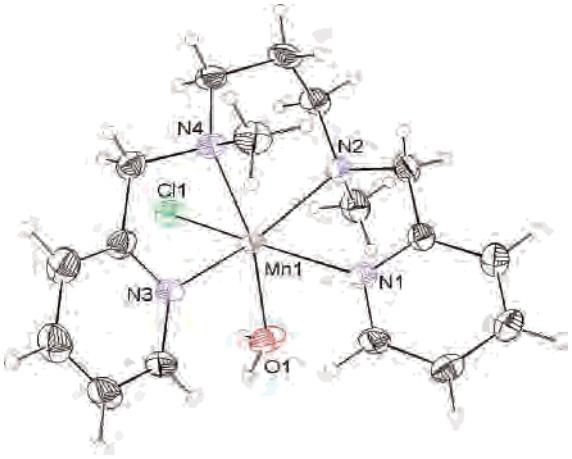

Figure 2. Molecular view of the cation **2**.

Table 3. Selected Bond Lengths (Å) and Angles (deg) for **2**

Mn−Cl1	2.468(1)	Mn−N2	2.296(4)
Mn−O1	2.194(4)	Mn−N3	2.257(4)
Mn−N1	2.311(3)	Mn−N4	2.326(4)
Cl1−Mn−N1	160.82(9)	N1−Mn−N2	73.6(1)
Cl1−Mn−N2	94.19(8)	N1−Mn−N3	98.5(1)
Cl1−Mn−N3	97.9(1)	N1−Mn−N4	102.6(1)
Cl1−Mn−N4	91.23(9)	N2−Mn−N3	158.3(1)
O1−Mn−N1	82.9(1)	N2−Mn−N4	87.1(1)
O1−Mn−N2	106.5(1)	N3−Mn−N4	74.7(1)
O1−Mn−N3	92.1(2)	Cl1−Mn−O	86.67(9)
O1−Mn−N4	166.3(1)		

environment. The Mn−Cl and Mn−N distances are similar to what is observed for Mn(II) complexes. Several ligand−metal−ligand angle values in **1** deviate significantly from the ideal value of 90° or 180° characteristic of a regular octahedron. However, all the angles measured in **1** fall in the range found for N_4Cl_2 mononuclear Mn(II) complexes.[58]

Crystal Structure of $[(L^3)MnCl(OH_2)](ClO_4)\cdot H_2O$ ($2(ClO_4)\cdot H_2O$). A view of cation **2** is presented in Figure 2, and principal bond lengths and angles are listed in Table 3. The Mn(II) ion is coordinated by the four nitrogen atoms of L^3, and two different exogenous ligands: one chloride anion and one water molecule. The latter are *cis* one another as are the two pyridine rings of L^3. Therefore, the L^3 ligand here presents the more unusual *cis*-β conformation. This may be related to a greater flexibility of L^3 compared to that of L^2, due to the propylene link in L^3 in place of the ethylene one in L^2. This change in the folding of the ligand on going from L^2 to L^3 has been previously observed with Fe(III). The structure of the cation $[(L^2)Fe(Cl)_2]^+$ is similar to that of **1**; in particular, the metal ion is coordinated by the four nitrogen atoms of the ligand, with the usual *cis*-α conformation, and by two exogenous chloride anions.[56] Similarly, the structure of the dinuclear complex $[(L^3)ClFe(\mu\text{-}O)Fe(Cl)_3]$ is reminiscent of that obtained for **2**, since the ligand coordinating the metal center is in a *cis*-β folding, the water molecule present there in **2** being replaced by the $\{(\mu\text{-}O)\text{-}Fe(Cl)_3\}$ motif.[56] The metal−ligand distances measured in **2** are similar to those reported in the literature. The ligand−metal−ligand angle values listed in Table 2 indicate that the Mn(II) ion in **2** is in a distorted octahedral geometry, as it is in **1**. The presence of a six-membered metallocycle in **2** versus a five-membered metallocycle in **1** does not seem to influence the distortion, contrarily to what is observed in **4** (see below). It is worth noting that only four other X-ray structures have been reported for hexacoordinated mononuclear Mn(II) complexes with four coordinated nitrogen atoms, one chloride anion, and one water molecule. Three of them concern the *cis*-$[(phen)_2MnCl(OH_2)]^+$ complex, the last one being the *cis*-$[(bpy)_2MnCl(OH_2)]^+$ cation. Similar deviations from the regular octahedron were observed.[59]

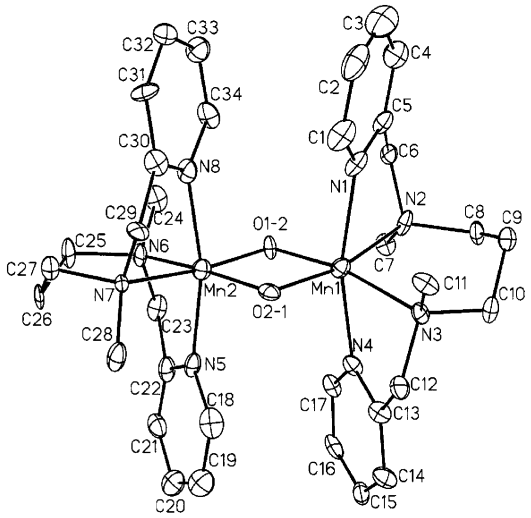

Figure 3. Molecular view of the cation **4**.

Crystal Structure of $[(L^3)Mn(\mu\text{-}O)_2Mn(L^3)](ClO_4)_3\cdot 3CH_3CN$ ($4(ClO_4)_3\cdot 3CH_3CN$). A view of cation **4** is presented in Figure 3, and principal bond lengths and angles are listed in Table 4. As observed previously for the analogous complex obtained with the ligand L^2,[16,60] the manganese ions are coordinated by two bridging oxos and the four nitrogen atoms of the ligand, the pyridine groups being in *trans* positions. Contrarily to the folding observed in complex **2**, the L^3 ligand here is in the more common *cis*-α conformation. From the values of the metal−ligand distances, one can identify the Mn1 and Mn2 sites as the Mn(III) and Mn(IV) ions, respectively. A comparison can be operated with crystallographic data reported in the literature for the complex $[(L^2)Mn(\mu\text{-}O)_2Mn(L^2)](ClO_4)_3\cdot H_2O$ ($\mathbf{3b}(ClO_4)_3\cdot H_2O$).[16] The Mn_2O_2 cores are very similar. However, the Mn···Mn separation is slightly higher in **4** (2.7242(11) vs 2.679(2) Å) due to the slight opening of the bridging angles Mn−O−Mn (97.08(10)° and 96.35(11)° in **4**, 94.5(2)° and 94.7(2)° in **3b**). The Mn(IV)−N_{pyr} distances are very similar in both complexes, while the Mn(III)−N_{pyr}

(58) Using the CCDC data, a total of 23 *cis*-Cl_2N_4 mononuclear Mn(II) complexes were selected with the following reference codes: ASOYIQ, GACSIM, GALMAH, GOSWOA, GUZLIW, HEVCEQ, HEZYEQ, HEZYIU, HUFDAN, IWOXUN, JIHLOB, MUPYUR, ODACUR, OHEDIO, QOFHUO, RECMOB01, RECMOB02, SASQAE, VAVBUP, XURZOZ, and ZECVOS. The references of the published structures are given in Table S1 in the Supporting Information.

(59) The CCDC references codes are IFUBUG, IFUCAN, IRONOS, and WINDOM. The references of the published structures are given in Table S2 in the Supporting Information.

(60) Hureau, C.; Blondin, G.; Cesario, M.; Un, S. *J. Am. Chem. Soc.* **2003**, *125*, 11637−11645.

Table 4. Selected Bond Lengths (Å) and Angles (deg) for **4**

Mn1−O1-2	1.838(2)	Mn2−O1-2	1.797(3)
Mn1−O2-1	1.858(3)	Mn2−O2-1	1.797(2)
Mn1−N1	2.211(4)	Mn2−N5	2.063(4)
Mn1−N4	2.170(4)	Mn2−N8	2.064(4)
Mn1−N2	2.198(3)	Mn2−N6	2.182(3)
Mn1−N3	2.158(3)	Mn2−N7	2.152(3)
Mn1···Mn2	2.7242(11)		
O1-2−Mn1−O2-1	81.87(11)	O1-2−Mn2−O2-1	84.71(11)
O1-2−Mn1−N1	96.64(12)	O1-2−Mn2−N5	97.14(13)
O1-2−Mn1−N4	94.79(12)	O1-2−Mn2−N8	93.76(13)
O1-2−Mn1−N2	88.89(11)	O1-2−Mn2−N6	87.92(12)
O1-2−Mn1−N3	168.97(13)	O1-2−Mn2−N7	169.84(13)
O2-1−Mn1−N1	94.79(13)	O2-1−Mn2−N5	92.60(12)
O2-1−Mn1−N4	94.71(13)	O2-1−Mn2−N8	95.40(12)
O2-1−Mn1−N2	167.27(12)	O2-1−Mn2−N6	168.95(13)
O2-1−Mn1−N3	91.51(12)	O2-1−Mn2−N7	90.67(12)
N1−Mn1−N4	166.06(13)	N5−Mn2−N8	167.03(14)
N1−Mn1−N2	77.53(13)	N5−Mn2−N6	80.15(12)
N1−Mn1−N3	92.68(12)	N5−Mn2−N7	92.10(13)
N4−Mn1−N2	94.77(13)	N8−Mn2−N6	93.28(13)
N4−Mn1−N3	76.88(12)	N8−Mn2−N7	77.64(13)
N2−Mn1−N3	98.90(12)	N6−Mn2−N7	97.87(12)

distances are slightly shorter in **4** (2.211(4) and 2.170(4) Å in **4** vs 2.223(9) and 2.233(10) Å in **3b**). The Jahn−Teller distortion of the Mn(III) ion that develops along the $N_{pyr}-Mn-N_{pyr}$ direction is thus less pronounced with ligand L^3 than with L^2. But the main difference between the two complexes lies in the coordination of the amine functions. The $Mn-N_{amine}$ bond lengths are significantly longer in **4** than in **3b**, whatever the oxidation state of the Mn ion: 2.158(3), 2.198(3), 2.152(3), and 2.182(3) Å in **4** and 2.112(8), 2.151(8), 2.131(8), and 2.134(7) in **3b**, the first two concerning Mn(III) and the last two Mn(IV). The $N_{amine}-Mn-N_{amine}$ angles are also strongly different. In complex **4**, the values are 98.90(12)° and 97.87(12)° for the Mn1 and Mn2 sites, respectively, while they only reach 84.1(3)° and 83.4(3)° in **3b**. A six-membered metalloring, CCCNMnN, is only found in $Mn^{III}(\mu\text{-}O)_2Mn^{IV}$ core complexes when the ligand is 1,4,8,11-*N*,*N*′,*N*″,*N*‴-tetraazacyclotetradecane. In these cases, the measured $N_{amine}-Mn-N_{amine}$ angle values are smaller (average 85.1°), probably because of the macrocyclic effect of the ligand.[61]

Characterization of *cis*-[(L^2)Mn(Cl)$_2$] (1) and [(L^3)MnCl(OH$_2$)]$^+$ (2) upon Dissolution in Acetonitrile. EPR Spectroscopy. X-band (9.4 GHz) EPR spectra of frozen acetonitrile millimolar solutions of **1** (Figure 4a) and **2** (Figure 4b) were recorded at 10 K using the conventional perpendicular detection mode. Both spectra present features between 0 and 800 mT.

The signal recorded on the frozen solution of **1** can indeed be interpreted as originating from a system where the zero-field splitting (ZFS) effect and the Zeeman interaction are competitive.[40,62] Furthermore, packets of six well-resolved hyperfine lines are clearly detected on the $g_{eff} = 8.32$ and $g_{eff} = 5.12$ transitions of the EPR spectrum of **1** (see the inset of Figure 4a). These lines are issued from the hyperfine interaction of the $I = 5/2$ Mn nuclear spin with the $S = 5/2$ electronic spin. The number of lines and the spacing between them (8.5 mT) clearly evidence the mononuclearity of complex **1** in solution.[63] This demonstrates the maintenance upon dissolution of the mononuclear character of complex **1**.

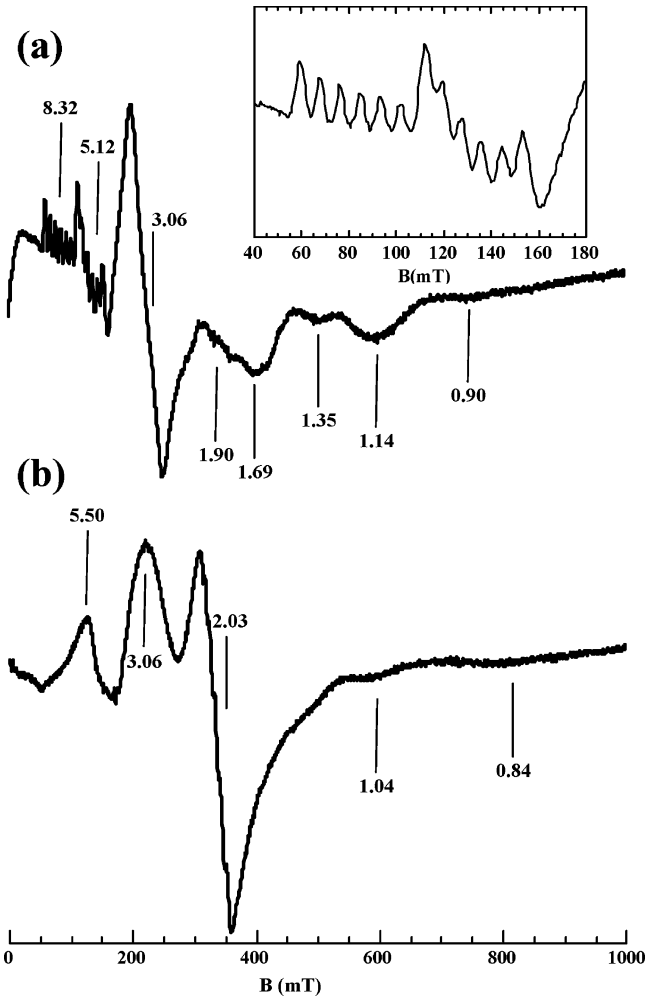

Figure 4. X-band EPR spectra of **1** (a) and **2** (b) recorded on millimolar acetonitrile solutions containing 0.1 M tetrabutylammonium perchlorate. Recording conditions: 0.5 mT modulation amplitude, 100 kHz modulation frequency, $T = 10$ K, 0.030 mW microwave power, $\nu = 9.38$ GHz. Inset: zoom of the 40−180 mT domain of spectrum a.

The signal recorded on a frozen solution of **2** cannot be interpreted in a similar straightforward manner. It can be noticed from the comparison with spectrum a that spectrum b exhibits transition with a larger line width. In addition weaker transitions are detected above 500 mT, and a more intense line is observed at 330 mT ($g_{eff} = 2$). Moreover, no Mn hyperfine structure is evidenced, whatever the concentration of the sample. The lack of Mn hyperfine structure is indicative of the presence in solution of chemically related Mn(II) complexes and/or a structural heterogeneity that would induce a distribution in the ZFS and hyperfine parameters. The substitution of the initially coordinated water

(61) The CCDC reference codes are KEZKUV, KEZLAC, SEJXUA, and YEJHIE. The references of the published structures are given in Table S3 in the Supporting Information.

(62) Bucher, C.; Duval, E.; Barbe, J.-M.; Verpeaux, J.-N.; Amatore, C.; Guilard, R.; Le Pape, L.; Latour, J.-M.; Dahaoui, S.; Lecomte, C. *Inorg. Chem.* **2001**, *40*, 5722−5726.

(63) Weil, J. A.; Bolton, J. R.; Wertz, J. E. *Electron Paramagnetic Resonance*. Wiley-Interscience: New York, 1994.

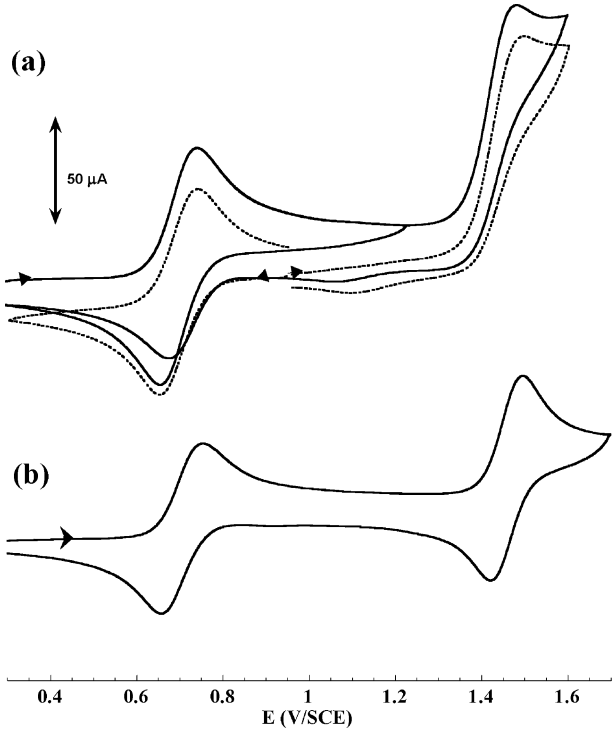

Figure 5. Cyclic voltammograms of a 5 mM acetonitrile solution of **1** in the presence of 0.1 M tetrabutylammonium perchlorate before (solid line) and after (dashed line) complete bulk electrolysis at $E = 1.0$ V vs SCE: (a) $T = 20$°C, scan rate 100 mV·s^{-1}, (b) $T = -30$°C, scan rate 100 mV·s^{-1}.

Table 5. $E_{1/2}$ (ΔE_P) and E_P Potential Values for **1**−**4**[a]

	Mn(II)/ Mn(III)	Mn(III)/ Mn(IV)	Mn_2(III,III)/ Mn_2(III,IV)	Mn_2(III,IV)/ Mn_2(IV,IV)
1	0.74 (0.070)	1.46 (0.075)		
2	0.81 (0.090)[b]	1.65		
3b			0.20 (0.100)	1.12 (0.105)
3a			0.26, 0.03	1.12 (0.090)
4[c]			0.32, 0.07	1.25 (0.095)

[a] Potentials are given in volts vs SCE. [b] Values corresponding to the $[(L^3)Mn(Cl)_2]^{0/+}$ couple. [c] Values collected for the in situ electrochemically prepared complex.

molecule by acetonitrile together with the greater flexibility of ligand L^3 in comparison with that of L^2 may explain these conclusions.

Cyclic voltammetry of 1 in acetonitrile solution at room and low temperature is presented in Figure 5 (see Table 5). Two oxidation processes are detected. The first one ($E_{1/2} = 0.74$ V vs SCE) is reversible ($\Delta E_P = 70$ mV).[64] At room temperature, the second one ($E_{Pa} = 1.55$ V vs SCE) is not, but lowering the temperature to −30 °C allows the reversibility at $E_{1/2} = 1.46$ V vs SCE ($\Delta E_P = 75$ mV) to be recovered. It is worth noting that the oxidation process of free chloride ions was not detected ($E_{Pa} = 1.3$ V vs SCE). Consequently, the two oxidation processes at $E_{1/2} = 0.74$ V vs SCE and $E_{1/2} = 1.46$ V vs SCE are assigned to the successive one-electron abstraction from *cis*-$[(L^2)Mn^{II}(Cl)_2]$, leading to $[(L^2)Mn^{III}(Cl)_2]^+$, and from $[(L^2)Mn^{III}(Cl)_2]^+$, generating $[(L^2)Mn^{IV}(Cl)_2]^{2+}$. The absence of reversibility of the second process at room temperature is due to the potential high reactivity of the Mn(IV) cation. At low temperature (−30 °C), the reactivity is slowed, thus allowing the reversibility of the second oxidation process to be observed (Figure 5b).

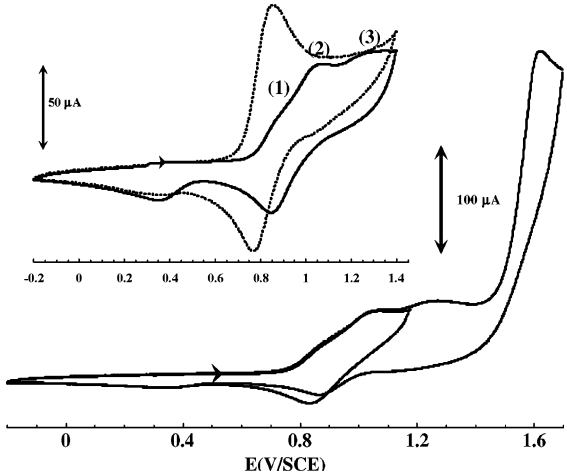

Figure 6. Cyclic voltammograms of a 5 mM acetonitrile solution of **2** in the presence of 0.1 M tetrabutylammonium perchlorate ($T = 20$ °C, scan rate 100 mV·s^{-1}). Inset: with (dashed line) or without (solid line) 1 equiv of tetraethylammonium chloride per molecule of **2**.

Room temperature cyclic voltammetry results of an acetonitrile solution of **2** are presented in Figure 6 (see Table 5). The anodic scan displays three successive peaks of similar intensity at $E_{Pa} = 0.8$, 1.1, and 1.3 V vs SCE. The inset of Figure 6 shows the evolution of the cyclic voltammogram upon addition of 1 equiv of chloride ions. The first peak (peak 1) increases in intensity and becomes reversible ($E_{1/2} = 0.81$ V vs SCE, $\Delta E_P = 90$ mV), while peaks 2 and 3 disappear. Moreover, the addition of 1 equiv of silver perchlorate salt to the original solution results in the disappearance of the three peaks and the appearance of a new one at 1.4 V vs SCE (Figure S1 in the Supporting Information). The presence of three oxidation processes in the potential range of 0.8−1.3 vs SCE suggests that ligand exchange occurs upon dissolution of **2**. From the similarity with the electrochemical behavior of complex **1**, we propose that the first oxidation process at $E_{1/2} = 0.81$ V vs SCE corresponds to the one-electron oxidation of $[(L^3)Mn^{II}(Cl)_2]$, leading to $[(L^3)Mn^{III}(Cl)_2]^+$. The attribution of peaks 2 and 3 is more uncertain. On the basis of the potential values and the evolution of the voltammogram upon addition of equivalents of silver ions, we propose that peaks 2 and 3 can be attributed to the monomeric cation $[(L^3)Mn^{II}Cl(S)]^+$, where S stands for a solvent molecule, and to a dinuclear chloro-bridged species, respectively.[65] The fourth peak appearing at $E_P = 1.4$ V vs SCE in the total absence of chloride anion is attributed to the dication $[(L^3)Mn^{II}(S)_2]^{2+}$, which would indeed be oxidized at a higher potential than the previously mentioned mononuclear monocationic Mn complexes. An additional intense oxidation peak is observed at $E_P = 1.65$ V vs SCE, which is attributed to a Mn(III)/ Mn(IV) oxidation process.

(64) $E_{1/2}$ is defined as $^1/_2(E_{Pa} + E_{Pc})$, and $E_P = |E_{Pa} - E_{Pc}|$, where E_{Pa} (E_{Pc}) is defined as the potential of the maximum of the current intensity when scanning is done toward anodic (cathodic) potentials.

(65) Romero, I.; Collomb, M.-N.; Deronzier, A.; Llobet, A.; Perret, E.; Pécaut, J.; Le Pape, L.; Latour, J.-M. *Eur. J. Inorg. Chem.* **2001**, 69−72.

Scheme 1

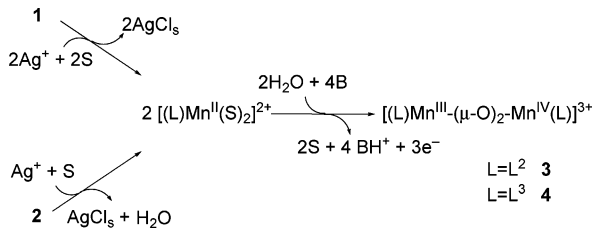

Electrochemical Conversion of 1 and 2 into Di-μ-oxo Core Dinuclear Mixed-Valent Complexes [(L)Mn^{III}-(μ-O)$_2$^{IV}Mn(L)]$^{3+}$. In the following paragraph, we will describe how di-μ-oxo dinuclear complexes can be generated from the above-mentioned Mn(II) species **1** and **2**. The general principle has already been illustrated with related Mn(II) complexes.[32,40] In the present investigation, the first step consists of the precipitation of the chloride ions by addition of a stoichiometric quantity of silver perchlorate to a solution of **1** (respectively **2**), thus generating the corresponding mononuclear Mn(II) complexes $[(L^2)Mn(S)_2]^{2+}$ (respectively $[(L^3)Mn(S)_2]^{2+}$), where S stands for either an acetonitrile or a water solvent molecule. The silver chloride precipitate is filtrated. The second step is the bulk electrolysis of the in situ generated complexes, in the presence of 2 equiv per Mn ion of an appropriate base. Here we use 2,6-dimethylpyridine. The complete chemical/electrochemical sequence is summarized in Scheme 1.

Figure 7a shows the cyclic voltammogram recorded on the $[(L^2)Mn(S)_2]^{2+}$ species in the presence of 2 equiv of base per Mn ion in acetonitrile solution (dashed line). The oxidation process at E_P = 1.2 V vs SCE takes place at a higher potential than that observed for the bischloro complex **1**. This is expected when the anionic chloride ligands are replaced by neutral molecules (water or solvent). In contrast with the reversible oxidation process of complex **1**, the Mn(II)/Mn(III) oxidation process is now irreversible. This was reported previously[40] for a related complex obtained with a hexadentate aminopyridine ligand, and it was proposed that the irreversibility arises from the deprotonation of a coordinated water molecule at the Mn(III) oxidation state.

Electrolysis has been performed at 1.2 V vs SCE. The completion is realized after the consumption of 1.5 e$^-$ per Mn ion, and the whole evolution of the transformation was characterized by cyclic voltammetry and UV−vis and EPR spectroscopies.

UV−Vis, EPR, and IR Characterizations of 3a and 4. Aliquots of the solution were collected during bulk electrolysis and UV−vis and EPR spectra recorded. The UV−vis spectrum of **1** is featureless, as expected for Mn(II) species. During the course of the electrolysis, three bands appear in the visible region at 453, 554, and 650 nm and increase continuously. The ϵ values have been calculated for the spectrum recorded after the completion of the electrolysis and are summarized in Table 6. These values agree with those observed for the chemically prepared compound **3b**$(ClO_4)_3$.[16,66]

The 100 K EPR spectra recorded during the course of the electrolysis are presented in Figure 8. The initial spectrum

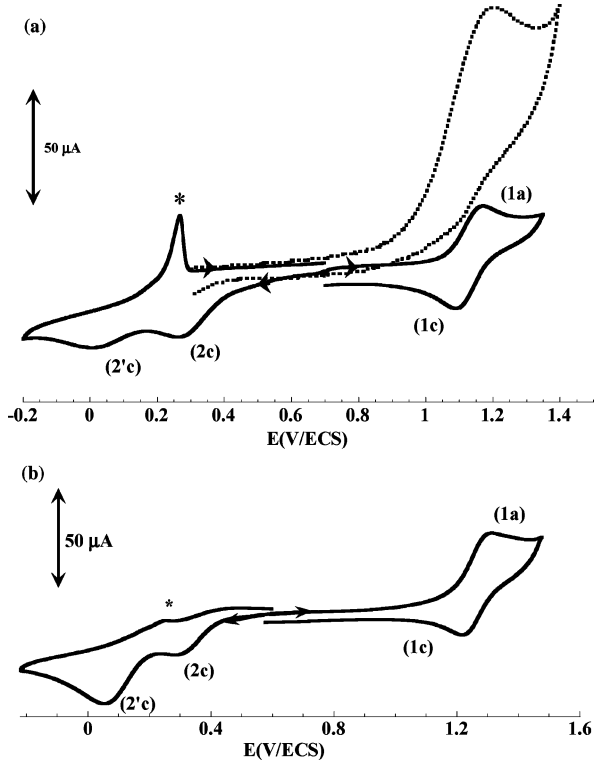

Figure 7. Cyclic voltammograms (T = 20 °C, scan rate 100 mV·s^{-1}) of a 5 mM acetonitrile solution with 0.1 M tetrabutylammonium perchlorate of (a) **1** after addition of 2 equiv of silver perchlorate and filtration, followed by addition of 2 equiv of 2,6-lutidine [before electrolysis (dashed line), after complete bulk electrolysis at E = 1.2 V vs SCE (solid line)] and (b) **2** after addition of 1 equiv of silver perchlorate and filtration, followed by addition of 2 equiv of 2,6-lutidine and complete bulk electrolysis at E = 1.4 V vs SCE (solid line). The asterisk indicates the redissolution peak of Ag.

Table 6. UV−Vis Data for Complexes **3**−**6** Electrochemically Prepared[a]

complex	λ (nm) (ϵ, M^{-1}·cm^{-1})	λ (nm) (ϵ, M^{-1}·cm^{-1})	λ (nm) (ϵ, M^{-1}·cm^{-1})
3	453 (435)	554 (209)	650 (174)
4	440 (460)	545 (250)	656 (250)
5	394 (1150)	500 (300)	536 (360)
6[b]	430	547	621

[a] The ϵ values are given per Mn ion. [b] The ϵ values are not mentioned since the electrochemical preparation from **2** is not quantitative.

presents three main transitions at g_{eff} = 5.7, 2.9, and 2. Hyperfine lines are observed on the g_{eff} = 2 transition and are separated by 8.5 mT. The profile evidences a high-spin mononuclear Mn(II) species.[67] In addition, this complex presents a reduced ZFS effect compared to that of **1**. This is in agreement with the substitution of the two chloride anions by either water or acetonitrile molecules that are characterized by a stronger ligand field strength. Indeed the D parameter of the ZFS is inversely proportional to the ligand field strength (ref 68 and references therein). The intensity of this signal decreases concomitantly with the appearance

(66) The chemical synthesis of **3b**$(ClO_4)_3$ has already been reported in the literature. In this work, we reproduced it for direct comparison with the electrochemically generated one.

(67) Garribba, E.; Micera, G.; Zema, M. *Inorg. Chim. Acta* **2004**, *357*, 2038−2048.

(68) Mantel, C.; Baffert, C.; Romero, I.; Deronzier, A.; Pécaut, J.; Collomb, M.-N.; Duboc, C. *Inorg. Chem.* **2004**, *43*, 6455−6463.

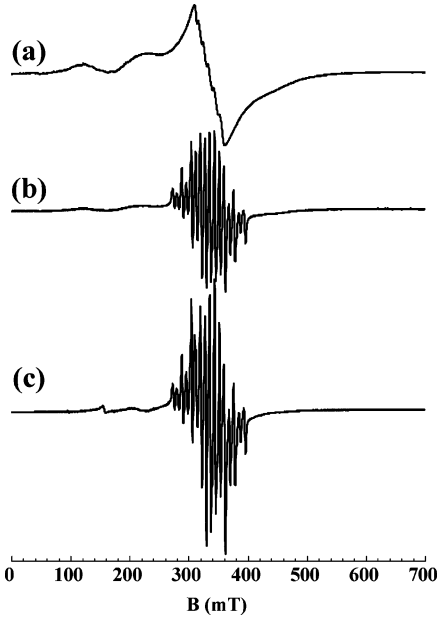

Figure 8. Evolution of the X-band EPR spectra during bulk electrolysis at $E = 1.2$ V vs SCE of a 5 mM acetonitrile solution of **1** containing 0.1 M tetrabutylammonium perchlorate after addition of 2 equiv of silver perchlorate, filtration, and addition of 2 equiv of 2,6-lutidine: (a) before electrolysis, (b) after exchange of 0.62 e^-/mol of **1**, (c) after exchange of 1.25 e^-/mol of **1**. Recording conditions: 0.5 mT modulation amplitude, 100 kHz modulation frequency, $T = 100$ K, 2.0 mW microwave power, $\nu = 9.38$ GHz.

of a new multiline signal centered at $g_{eff} = 2$. This signal spread over a 124 mT range (first peak to last trough) and presents 16 lines regularly spaced by about 8 mT, highly characteristic of the mixed-valent Mn_2(III,IV) di-μ-oxo core.[69,70]

When bulk electrolysis is performed on a highly concentrated (10 mM) solution of **1**, the electrolyzed product could be isolated as a powder. The IR spectrum of this powder exhibits the same bands as complex **3b**$(ClO_4)_3$ independently chemically prepared. The EPR spectrum recorded on an acetonitrile solution of this powder can be exactly superimposed on the spectrum shown in Figure 8c. This spectrum was simulated (Figure S2 in the Supporting Information), and the parameters are reported in Table 8. We did not attempt crystallization since the X-ray structure of the complex has already been described with several counterions.[16,60]

These three characterizations demonstrate unambiguously that the bulk electrolysis of *cis*-$[(L^2)Mn(Cl)_2]$ after removal of chloride ions and in the presence of 2 equiv of 2,6-lutidine per Mn ion leads to the formation of the dinuclear mixed-valent complex $[(L^2)Mn^{III}(\mu\text{-}O)_2Mn^{IV}(L^2)]^{3+}$ **(3a)**. Moreover, this electrochemical preparation is quantitative according to the coulometric measurements and UV−vis spectra.

Identical experiments were performed with compound **2** as a starting material, and the formation of the complex $[(L^3)Mn^{III}(\mu\text{-}O)_2Mn^{IV}(L^3)]^{3+}$ (**4**) was evidenced by EPR

Scheme 2

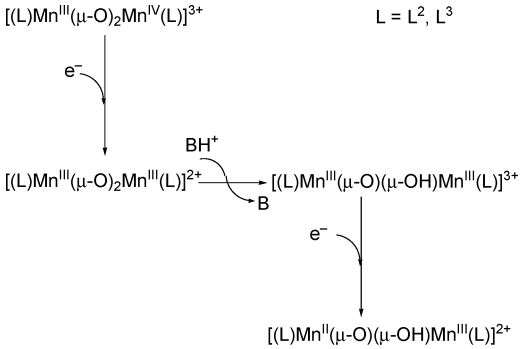

(Figure S3 in the Supporting Information) and UV−vis spectroscopies (see Table 6). The EPR spectrum recorded on an acetonitrile solution of recrystallized complex **4** (Figure 12b) displays the characteristics of the now well-known signature of a di-μ-oxo-Mn_2(III,IV) core. Furthermore, the two EPR signatures recorded at the end of the bulk electrolysis and of the dissolved crystals of **4** can be superimposed. Simulation parameters are reported in Table 8. They are very similar to those of **3a** and will be discussed further in the text.

Cyclic Voltammetry of in Situ Generated Complexes 3a and 4. The cyclic voltammogram recorded after bulk electrolysis of $[(L^2)Mn(S)_2]^{2+}$ in the presence of 2 equiv of 2,6-lutidine per Mn ion, at $E = 1.2$ V vs SCE, is presented in Figure 7a (solid line). One reversible oxidation wave (wave 1) is detected at $E_{1/2} = 1.12$ V vs SCE ($\Delta E_P = 90$ mV) when scanning is done toward anodic potentials, and two irreversible waves (waves 2c and 2′c; see Figure 7a) are respectively detected at $E_P^{2c} = 0.26$ and $E_P^{2'c} = 0.03$ V vs SCE when scanning is done toward cathodic potentials (see Table 5). One additional irreversible cathodic peak is observed at $E_p = -1.5$ V vs SCE (data not shown). We checked that this peak corresponds to the reduction of the protonated 2,6-lutidine. Wave 1 is identical to that observed for the chemically prepared dinuclear complex $[(L^2)Mn^{III}(\mu\text{-}O)_2Mn^{IV}(L^2)]^{3+}$ (**3b**) and corresponds to the Mn_2(III,IV) to Mn_2(IV,IV) oxidation process.[16] In place of the expected reversible Mn_2(III,IV)/Mn_2(III,III) cathodic process, usually observed at $E_{1/2} = 0.20$ V vs SCE for a solution of the chemically prepared **3b**$(ClO_4)_3$, two cathodic peaks are recorded (peaks 2c and 2′c). The difference between the two cyclovoltammograms is unambiguously due to different solution compositions. Indeed, the presence of additional protonated 2,6-lutidine is unavoidable at the end of the electrolysis experiment and specific to it. The cathodic signature could be explained considering the successive electrochemical and chemical reactions described below and presented in Scheme 2. The cathodic potential of peak 2c is slightly higher than the $E_P = 0.16$ V vs SCE value detected for chemically prepared **3b**$(ClO_4)_3$. The difference in potential values and the absence of reversibility, even when scanning is done down to 0.15 V vs SCE (data not shown), are in agreement with a chemical reaction following the electrochemical reduction of $[(L^2)Mn^{III}(\mu\text{-}O)_2Mn^{IV}(L^2)]^{3+}$ into $[(L^2)Mn^{III}(\mu\text{-}O)_2Mn^{III}(L^2)]^{2+}$. Since protonated 2,6-lutidine is present in solution, we propose that the implied chemical

(69) Cooper, S. R.; Dismukes, G. C.; Klein, M. P.; Calvin, M. *J. Am. Chem. Soc.* **1978**, *100*, 7248−7252.
(70) Schäfer, K.-O.; Bittl, R.; Zweygart, W.; Lendzian, F.; Haselhorst, G.; Weyhermüller, T.; Wieghardt, K.; Lubitz, W. *J. Am. Chem. Soc.* **1998**, *120*, 13104−13120.

Table 7. Estimated pK_a Values of the Closely Related Complex $[(bispicen)Mn^{III}(\mu\text{-}O)_2Mn^{III}(bispicen)]^{3+}$, Where bispicen is *N*,*N*′-Bis(2-pyridylmethyl)ethane-1,2-diamine, and for 2,6-Lutidine

acid/base couple	pK_a	ref
$[(bispicen)Mn^{III}(\mu\text{-}O)(\mu\text{-}OH)Mn^{III}(bispicen)]^{3+}$/ $[(bispicen)Mn^{III}(\mu\text{-}O)_2Mn^{III}(bispicen)]^{2+}$	16[a]	71, 72
2,6-lutidineH^+/2,6-lutidine	14	73
$[(bispicen)Mn^{III}(\mu\text{-}OH)_2Mn^{III}(bispicen)]^{4+}$/ $[(bispicen)Mn^{III}(\mu\text{-}O)(\mu\text{-}OH)Mn^{III}(bispicen)]^{3+}$	8[b]	74

[a] A value of 8.35 has been measured in water.[71] The pK_a = 16 value was calculated according to the relation $pK_a(CH_3CN) = pK_a(H_2O) + 7.5$.[72] [b] This p$K_a$ value was estimated considering that for a di-μ-oxo complex the two pK_a values are spaced by about 8 pK_a units.[74]

Table 8. Parameters of the EPR Simulations Performed with Rhombic and Collinear Tensors[a]

		g	$\lvert A_1\rvert$	$\lvert A_2\rvert$
3b	*x*[b]	1.999	0.0161	0.0070
	y	1.995	0.0147	0.0072
	z	1.983	0.0110	0.0075
	iso	1.993	0.0140	0.0072
4	*x*	2.001	0.0162	0.0068
	y	1.996	0.0150	0.0073
	z	1.985	0.0115	0.0076
	iso	1.994	0.0142	0.0072
6	*x*	2.007	0.0146	0.0072
	y	2.004	0.0134	0.0071
	z	1.990	0.0106	0.0078
	iso	2.000	0.0129	0.0074

[a] Hyperfine coupling constants are given in cm^{-1}. [b] The *x*, *y*, and *z* labels refer to the *g* principal values ordered in decreasing order. The label *iso* denotes the isotropic component calculated as one-third of the sum of the three principal values.

reaction is the protonation of one of the oxo bridges, leading to $[(L^2)Mn^{III}(\mu\text{-}O)(\mu\text{-}OH)Mn^{III}(L^2)]^{3+}$. This is expected when the pK_a values reported for protonated species issued from $[(bispicen)Mn^{III}(\mu\text{-}O)_2Mn^{III}(bispicen)]^{2+}$, a complex closely related to **3a**, and listed in Table 7 are considered. In such a case, the second electrochemical process would be the reduction of $[(L^2)Mn^{III}(\text{-}\mu\text{-}O)(\mu\text{-}OH)Mn^{III}(L^2)]^{3+}$ thus generated. The resulting Mn(II)Mn(III) species is probably not stable as a dinuclear complex.

The cyclic voltammogram recorded on a solution of **2** containing 1 equiv of silver per chlorate and 2 equiv of 2,6-lutidine presents a feature similar to that of complex **1** prepared in identical conditions (see Figure S4 in the Supporting Information). Figure 7b shows the cyclic voltammograms recorded after exhaustive bulk electrolysis (1.5 e^- per Mn) of this solution. They are pretty similar to those shown in Figure 7a (see also Table 5). This further confirms the formation of $[(L^3)Mn^{III}(\mu\text{-}O)_2Mn^{IV}(L^3)]^{3+}$ (**4**). The irreversibility of the cathodic processes supports the successive electrochemical and chemical reactions described in Scheme 2. A definitive proof of the formation of **4** was the growth of crystals suitable for X-ray diffraction studies.

It has to be noticed that several di-μ-oxo-bridged high-valent Mn dinuclear complexes with related tetradentate aminopyridine ligands have been systematically synthesized using hydrogen peroxide in alkaline medium and X-ray characterized. The complex with L^3 is missing in this series. Preparation of **4** by the same chemical procedure was always thwarted. It is then remarkable that using the electrochemical route, we succeed in growing crystals of **4** (see the

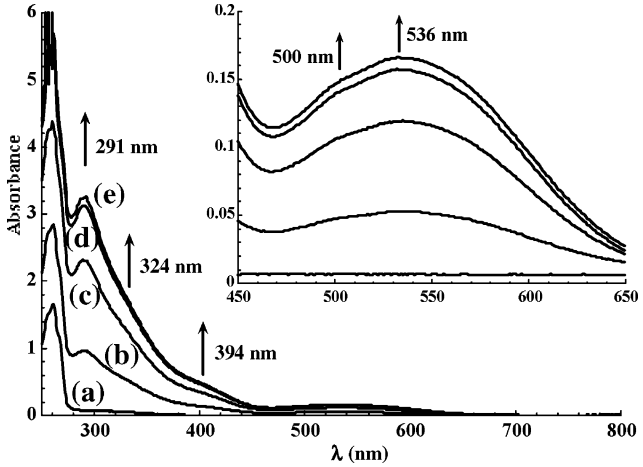

Figure 9. Evolution of the UV−vis spectrum of **1** (4.6 mM) during bulk electrolysis at E = 1.0 V vs SCE of an acetonitrile solution containing 0.1 M tetrabutylammonium perchlorate: (a) before electrolysis, (b) after exchange of 0.23 e^-/mol of **1**, (c) after exchange of 0.69 e^-/mol of **1**, (d) after exchange of 0.92 e^-/mol of **1**, (e) after exchange of 1 e^-/mol of **1** (T = 20 °C, l = 1 mm).

Experimental Section). In **4**, the folding of L^3 is *cis*-α, thus implying a conformational change in the course of the electrolysis.

Electrochemical Oxidation of 1 and 2(ClO_4). Influence of Chloride Anions. Chloride anions are proposed to play an important role in the OEC function. As a consequence, it is of interest to study the electrochemical oxidation of complexes **1** and **2**(ClO_4) in the presence of chloride anions. As anticipated in view of the difference in the cyclic voltammetry signatures of the two complexes (see Figures 5 and 6), the resulting products after electrolysis should be dramatically different. Indeed, for complex **1**, the formation of the one-electron oxidation product $[(L^2)Mn^{III}(Cl)_2]^+$ is expected, whereas, for complex **2**, one cannot easily foresee the result.

Bulk Electrolysis of 1. Bulk electrolysis was performed on a solution of **1** at E = 1.0 V vs SCE, and the coulometric measurements indicated a one-electron process. Figure 5a presents the cyclic voltammogram recorded on the electrolyzed solution (dashed line). Starting the scan from 1.0 V vs SCE, one reversible wave at $E_{1/2}$ = 0.74 V vs SCE (respectively one irreversible wave at E_P = 1.55 V vs SCE) is recorded when scanning is done toward cathodic (respectively anodic) potentials: both are identical to those recorded on the starting Mn(II) solution of **1**. These signatures unambiguously indicate that the compound obtained is the expected cation $[(L^2)Mn^{III}Cl_2]^+$.

During the course of the electrolysis, aliquots of the solution were collected and UV−vis and EPR spectra recorded. The evolution of the UV−vis spectrum is presented in Figure 9. Three principal bands are detected in the visible region at λ = 394, 500, and 536 nm, and the extinction coefficients value ϵ summarized in Table 6 have been calculated from the spectrum recorded after the completion of the electrolysis. The transition detected at λ = 394 nm (1150 $M^{-1}\cdot cm^{-1}$) is assigned to a $Cl^- \rightarrow$ Mn(III) LMCT (ligand to metal charge transfer) transition on the basis of the reported values for other Mn(III) complexes bearing

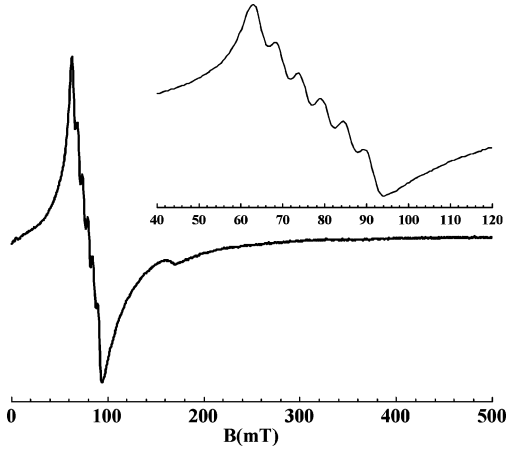

Figure 10. X-band parallel mode spectrum of a 5 mM acetonitrile solution of **1** after one-electron oxidation at $E = 1.0$ V vs SCE. Recording conditions: 0.5 mT modulation amplitude, 100 kHz modulation frequency, $T = 5$ K, 2.0 mW microwave power, $\nu = 9.42$ GHz.

nitrogen-containing ligands.[75−77] The transitions observed at 500 and 536 nm are attributed to d−d Mn(III) transitions, in agreement with the low extinction coefficients theoretically expected for d−d transitions.[78,79]

The evolution of the EPR spectrum, recorded in the conventional perpendicular mode, shows the progressive disappearance of the signature of **1**. The lack of an X-band perpendicular detection mode EPR signal for the one-electron-electrolyzed solution is strongly indicative of the formation of a Mn(III) species. Indeed high-spin Mn(III) complexes are known to present a strong zero-field splitting effect due to the Jahn−Teller distortion. On the other hand, the X-band parallel mode EPR spectrum of the complete electrolyzed solution exhibits six well-resolved hyperfine lines centered at $g_{eff} = 8.6$ and spaced by 6.2 mT as presented in the inset of Figure 10. These lines are a clear demonstration of the formation of a mononuclear high-spin Mn(III) complex.[80−84] As previously described in the literature, X-band parallel mode EPR spectra are expected for an $S =$ 2 system with a strong ZFS splitting with symmetry close to axiality.[85,86] The short hyperfine line separation indicates that the Jahn−Teller distortion is an elongation.[82,87]

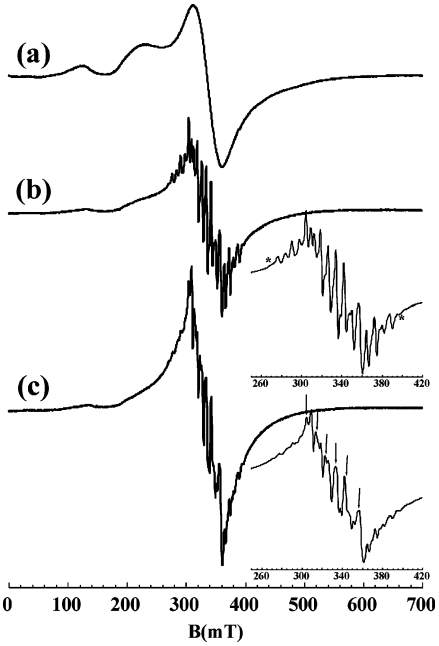

Figure 11. Evolution of the X-band EPR spectrum of **2** (5 mM) during bulk electrolysis at $E = 1.2$ V vs SCE in acetonitrile solution containing 0.1 M tetrabutylammonium perchlorate: (a) before electrolysis, (b) after exchange of 0.6 e^-/mol of **2**, (c) after exchange of 1.1 e^-/mol of **2**. Recording conditions: 0.5 mT modulation amplitude, 100 kHz modulation frequency, $T = 100$ K, 2.0 mW microwave power, $\nu = 9.38$ GHz.

In conclusion, the one-electron oxidation of complex **1** leads as expected to the formation of the mononuclear species $[(L^2)Mn^{III}(Cl)_2]^+$ (**5**). We will show in the following section that the electrochemical oxidation of complex **2** is a more knotty point.

Bulk Electrolysis of 2. Electrolysis of **2** was performed at 1.2 V vs SCE, and completed after consumption of 1.0 e^- per Mn ion. Aliquots of the solution were collected during the course of the electrolysis and EPR and UV−vis spectra recorded. Cyclic voltammetry recorded on the solution at the end of electrolysis did not allow the clear attribution of a unique species. Nevertheless, a clear and intense cathodic peak was observed at −1.7 V vs SCE, which is attributed to the reduction of the protonated ligand (data not shown).

UV−vis spectra recorded during the course of the electrolysis show the growth of bands at $\lambda_1 = 291$ nm, $\lambda_2 = 430$ nm, $\lambda_3 = 547$ nm, and $\lambda_4 = 621$ nm. These bands are somewhat similar to those usually observed for dinuclear di-μ-oxo-Mn_2(III,IV) complexes, but not identical to those reported in Table 5 for compound **4** (see Figure S5 in the Supporting Information).

However, evolution of the collected 100 K X-band EPR spectra is more informative (Figure 11). The initial spectrum of **2** is presented in Figure 11a and exhibits three main transitions at $g_{eff} = 5.5$, 2.9, and 2. Note that it differs from the spectrum of Figure 4b due to the difference in

(71) Manchanda, R.; Thorp, H. H.; Brudvig, G. W.; Crabtree, R. H. *Inorg. Chem.* **1991**, *30*, 494−497.
(72) Dubé, C. E.; Wright, D. W.; Armstrong, W. H. *J. Am. Chem. Soc.* **1996**, *118*, 10910−10911.
(73) Kaljurand, I.; Rodima, T.; Leito, I.; Koppel, I. A.; Schwesinger, R. *J. Org. Chem.* **2000**, *65*, 6202−6208.
(74) Baldwin, M. J.; Pecoraro, V. L. *J. Am. Chem. Soc.* **1996**, *118*, 11325−11326.
(75) Triller, M. U.; Pursche, D.; Hsieh, W.-Y.; Pecoraro, V. L.; Rompel, A.; Krebs, B. *Inorg. Chem.* **2003**, *42*, 6274−6283.
(76) Goodwin, H. A.; Sylva, R. N. *Aust. J. Chem.* **1965**, *18*, 1743−1749.
(77) Pascaly, M.; Duda, M.; Rompel, A.; Sift, B. H.; Meyer-Klaucke, W.; Krebs, B. *Inorg. Chim. Acta* **1999**, *291*, 289−299.
(78) Dingle, R. *Acta Chem. Scand.* **1966**, *20*, 33−44.
(79) Davis, T. S.; Fackler, J. P.; Weeks, M. J. *Inorg. Chem.* **1968**, *7*, 1994−2002.
(80) Dexheimer, S. L.; Gohdes, J. W.; Chan, M. K.; Hagen, K. S.; Armstrong, W. H.; Klein, M. P. *J. Am. Chem. Soc.* **1989**, *111*, 8923−8925.
(81) Campbell, K. A.; Yikilmaz, E.; Grant, C. V.; Gregor, W.; Miller, A.-F.; Britt, R. D. *J. Am. Chem. Soc.* **1999**, *121*, 4714−4715.
(82) Campbell, K. A.; Force, D. A.; Nixon, P. J.; Dole, F.; Diner, B. A.; Britt, R. D. *J. Am. Chem. Soc.* **2000**, *122*, 3754−3761.
(83) Campbell, K. A.; Lashley, M. R.; Wyatt, J. K.; Nantz, M. H.; Britt, R. D. *J. Am. Chem. Soc.* **2001**, *123*, 5710−5719.
(84) Maneiro, M.; Bermejo, M. R.; Fondo, M.; González, A. M.; Sanmartin, J.; Garcia-Monteagudo, J.-C.; Pritchard, R. G.; Tyryshkin, A. M. *Polyhedron* **2001**, *20*, 711−719.
(85) Hendrich, M. P.; Debrunner, P. G. *Biophys. J.* **1989**, *56*, 489−506.
(86) Krzystek, J.; Telser, J. *J. Magn. Reson.* **2003**, *162*, 454−465.
(87) Gerritsen, H. J.; Sabisky, E. S. *Phys. Rev.* **1963**, *132*, 1507−1512.

the recording temperature. This 100 K signal is strongly reminiscent of the transitions detected for the related $[(L^2)Mn(S)_2]^{2+}$ complex (see Figure 8a). This signal fades upon oxidation concomitantly with the appearance of a new multiline spectrum centered at $g_{eff} = 2$, with a 114 mT width (first peak to last trough). The observed modifications of the profile of the signal during the course of the electrolysis indicate the presence of several EPR-active species in solution. In particular, one shall notice the appearance of six additional hyperfine lines separated by 8.5 mT, centered at $g_{eff} = 2$. This signal is maximum at the end of the electrolysis (see the strokes in the inset of Figure 11c) and is typical of a solvated Mn(II) ion. Consequently, the spectra recorded are the superimposition of at least three different contributions in varying amounts, namely, the spectrum obtained upon dissolution of complex **2** (Figure 11a), the solvated Mn(II) signature, and the 114 mT wide multiline signal centered at $g_{eff} = 2$. This last signal presents hyperfine lines spaced by 7.2 mT, characteristic of a mixed-valent Mn_2(III,IV) oxo-bridged species that we shall note **6** in the following section. A thorough analysis of the spectra reveals the presence of two additional lines of very weak intensity that are indeed located at the same resonant field positions as the two outermost lines of the previously described multiline signal of **4** (see the asterisks in the inset of Figure 11b). These two lines are attributed to the presence of a small amount of complex **4** in the electrolyzed solution. Successive subtractions of the two Mn(II) species and of the complex **4** contributions (see the Experimental Section for details) in the spectrum recorded after the consumption of 0.6 e^-/mol of **2** (Figure 11b) allowed an EPR signature of **6** to be obtained. This resulting signature is suitable for the simulation process (Figure 12). Simulation has been performed using the commonly used hypotheses for such systems (see the Experimental Section). The parameters used are listed in Table 8. The **g** tensor presents a very small anisotropy. The $\mathbf{A}_1$ hyperfine tensor presents a rhombic symmetry, while the $\mathbf{A}_2$ hyperfine tensor is almost isotropic. As theoretically predicted for an $S = 1/2$ Mn(III)Mn(IV) system, the isotropic components of both hyperfine tensors are in a 2:1 ratio. Therefore, the subscripts 1 and 2 used in the description of the simulation are respectively assigned to the Mn(III) and Mn(IV) ions.

As reported before, the spectral width and profile are highly indicative of the nature of the dimanganese cores.[20,32,70] Whereas the 124 mT width of compound **4** is in total agreement with the formation of a di-μ-oxo bridge, the 114 mT width of compound **6** is strongly reminiscent of an unsupported mono-μ-oxo bridge.[20,32] The 0.0129 cm^{-1} value determined for the isotropic Mn(III) hyperfine component in **6** is indeed close to the 0.0127 and 0.0124 cm^{-1} values reported for the two mixed-valent mono-μ-oxo-bridged complexes described in the literature.[20,32] It is in fact significantly smaller than the 0.0140 and 0.0142 cm^{-1} values determined, for instance, for di-μ-oxo complexes **3a** and **4** (see Table 8).

As a consequence, we propose from the EPR data that compound **6** is a mono-μ-oxo mixed-valent dinuclear complex. Considering that the rare unsupported mono-μ-oxo-bridged complexes reported in the literature contain negatively charged ligands in the Mn coordination sphere,[20,23,32,34,45] we suggest that the chloride ions coordinated in the former complex **2** ensured this role. This assumption is enforced by the impossibility to synthesize complex **6** in the absence of chloride anions (see the Discussion). Complex **6** is subsequently proposed to be $[(L^3)ClMn^{III}(\mu\text{-}O)Mn^{IV}Cl(L^3)]^{3+}$. One shall notice that the similar $[ClM(\mu\text{-}O)MCl]^{2+}$ core has been obtained in the past with an N4 ligand and Fe(III)[88] or Mn(III).[34]

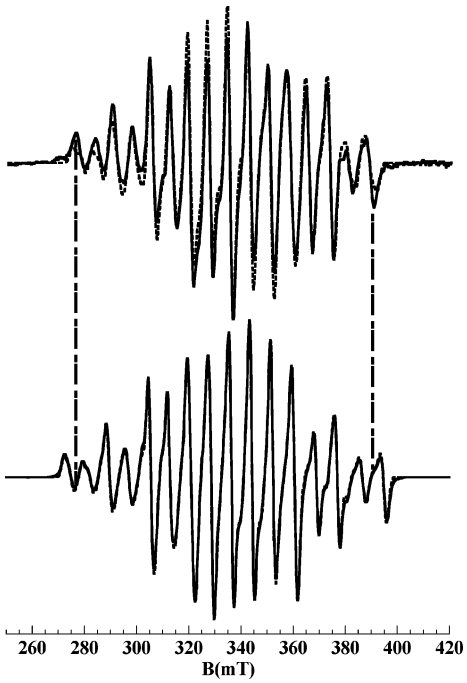

Figure 12. Experimental (solid line) and simulated (dashed line) X-band EPR spectra recorded on an acetonitrile solution containing 0.1 M tetrabutylammonium perchlorate: (a) $[(L^3)ClMn(\mu\text{-}O)MnCl(L^3)]^{3+}$ (**6**) and (b) $[(L^3)Mn(\mu\text{-}O)_2Mn(L^3)]^{3+}$ (**4**). Recording conditions: 0.5 mT modulation amplitude, 100 kHz modulation frequency, $T = 100$ K, 2.0 mW microwave power, $\nu = 9.386$ GHz. Simulation parameters: full width at half-height 1.2 mT (a), 1.1 mT (b); agreement factor $R = 0.062$ (a), 0.004 (b).

Discussion

The various experiments described above demonstrated that ligand L^3 offers access to two different di-manganese oxo-bridged species. We will discuss the role of chloride ions to generate the mono-μ-oxo complex as well as the influence of the external base. The difference in the propylene vs ethylene link in the tetradentate ligand will also be considered.

Formation of Di-μ-oxo Bridges. We have shown that the electrochemical oxidation of the mononuclear Mn(II) complexes **1** and **2** in the absence of chloride ions and in the presence of 2 equiv of an external base per Mn ion led to the formation of the di-μ-oxo dinuclear complexes $[(L)Mn^{III}(\mu\text{-}O)_2Mn^{IV}(L)]^{3+}$ ($L = L^2$ (**3**), $L = L^3$ (**4**)). Protonated 2,6-lutidine was systematically detected at the

(88) Nivorozhkin, A.; Anxolabéhère-Mallart, E.; Mialane, P.; Davidov, R.; Guilhem, J.; Cesario, M.; Audière, J.-P.; Girerd, J.-J.; Styring, S.; Schussler, L.; Seris, J.-L. *Inorg. Chem.* **1997**, *36*, 846−853.

Scheme 3

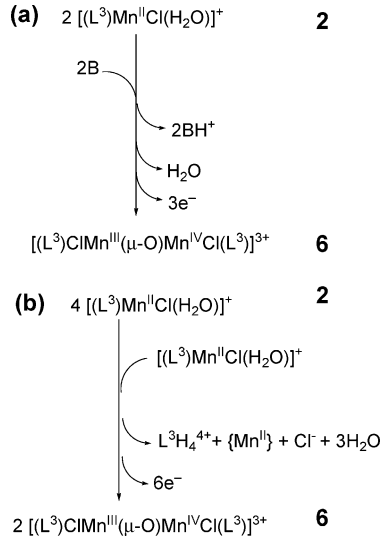

end of the electrolysis. In the absence of such a base, the formation of the dinuclear complexes $[(L)Mn^{III}(\mu\text{-}O)_2Mn^{IV}(L)]^{3+}$ was never observed. In the present case, the role of the base is thus to neutralize the protons generated by the building of the oxo bridges, originating from water molecules. It has been published in the literature that oxo-bridged Mn(III)Mn(IV) core complexes may result from the disproportionation between the analogous oxo-bridged and hydroxo-bridged Mn(III)Mn(III) species.[89] On the basis of these observations and readings, we propose that complexes **3** and **4** are issued from $[(L)Mn^{III}(\mu\text{-}O)_2Mn^{III}(L)]^{2+}$ and $[(L)Mn^{III}(\mu\text{-}O)(\mu\text{-}OH)Mn^{III}(L)]^{3+}$. According to the p$K_a$ values reported when L = bispicen (see Table 7), the two di-Mn(III) entities may indeed coexist in acetonitrile solution. These double-bridged species would result from successive condensation/deprotonation processes on mononuclear Mn(III) complexes generated upon electrochemical oxidation of the starting $[(L)Mn^{II}(S)_2]^{2+}$ species. However, we cannot exclude that complexes **3** and **4** are issued from the direct one-electron oxidation of the above-mentioned $[(L)Mn^{III}(\mu\text{-}O)_2Mn^{III}(L)]^{2+}$.

Formation of the Mono-μ-oxo Bridge. Whereas 2 equiv of base per Mn ion is required for the formation of di-μ-oxo species, only 1 equiv should be necessary to generate the mono-μ-oxo unit (Scheme 3a). Bulk electrolysis was thus performed in the presence of only 1 equiv of 2,6-lutidine per Mn ion to improve the yield of complex **6** that is indeed not quantitatively formed in the absence of base. Unfortunately the actual role of the base was to favor the formation of the di-μ-oxo bridge, as evidenced by EPR spectroscopy (Figure S6 in the Supporting Information). We equally attempt to run several electrolyses varying the amount of added base (0, 0.5, 1, or 2 equiv of base per Mn ion). EPR spectra were recorded during the courses of the four electrolyses. Scrupulous analysis of the four spectra recorded after the consumption of 0.6 e^- per Mn ion clearly shows that the quantity of the different species present in solution, namely, **2**, solvated Mn(II), **4**, and **6**, varies with the amount of added base (see Figure S6). In particular, when the amount of added base is increased, the quantity of di-μ-oxo-bridged complex **4** increases and the amount of solvated Mn(II) ion decreases concommitently. From these experiments, we propose that the formation of **6** is assisted by the ligand L^3 acting as a base (Scheme 3b). This is experimentally evidenced by the detection in the cyclic voltammogram of the electrolyzed solution of **2** of the reduction peak of the protonated L^3 ligand together with the recording of the EPR signature of solvated Mn(II) species. In fact, it has been previously reported for similar experiments that ligands can act as bases.[23,35−40,90] The building of the oxo bridges is thus intricately controlled by the competition between 2,6-lutidine and ligand L^3.

Bulk electrolyses in the absence or in the presence of 2,6-lutidine were also performed in the presence of 1 additional equiv of chloride ions, keeping in mind that this would hinder the formation of the second oxo bridge. Unfortunately all the electrochemical experiments attempted to quantitatively prepare compound **6** were unfruitful.

Different Behavior between L^2 and L^3. We have shown that the one-electron oxidation of the mononuclear complex **1** led to the quantitative formation of the cation $[(L^2)Mn(Cl)_2]^+$ (**5**). In contrast to this, when the bulk electrolysis of a solution of **2**(ClO_4) with a Mn:Cl = 1:2 ratio is performed, the quantitative formation of the similar $[(L^3)Mn(Cl)_2]^+$ compound is not observed. Cyclic voltammetry of the resulting solution (see Figure S7 in the Supporting Information), as well as EPR spectroscopy (see Figure S8 in the Supporting Information), evidenced the presence of three species, namely, the expected $[(L^3)Mn(Cl)_2]^+$ complex, the solvated Mn(II) species, and the mixed-valent mono-μ-oxo dinuclear $[(L^3)ClMn(\mu\text{-}O)MnCl(L^3)]^{3+}$ complex (**6**). Thus, the five-membered metalloring favors the formation of the $[(L^2)Mn(Cl)_2]^+$ complex, whereas the six-membered metalloring does not stabilize the mononuclear species $[(L^3)Mn(Cl)_2]^+$ in acetonitrile solution, which eventually evolves.

Moreover, it is worth noting that despite a lot of electrochemical attempts (varying the Cl:Mn and 2,6-lutidine:Mn ratios; see Figure S9 in the Supporting Information) on a solution of **1**, the complex analogous to **6**, namely, $[(L^2)ClMn(\mu\text{-}O)MnCl(L^2)]^{3+}$, has never been detected. The formation of the mixed-valent mono-μ-oxo dinuclear complex **6** is thus tightly related to the nature of complex **2**. In particular, the unusual *cis*-β folding of ligand L^3 and the presence of two different exogenous ligands may be proposed as determinant factors which favor such a mono-μ-oxo dinuclear system. One should notice that literature dealing with oxidation processes by either Fe[91] or Mn[92] complexes

(89) Wieghardt, K.; Bossek, U.; Nuber, B.; Weiss, J.; Bonvoisin, J.; Corbella, M.; Vitols, S. E.; Girerd, J.-J. *J. Am. Chem. Soc.* **1988**, *110*, 7398−7411.

(90) Pal, S.; Gohdes, J. W.; Wilisch, W. C. A.; Armstrong, W. H. *Inorg. Chem.* **1992**, *31*, 713−716.

(91) Raffard-Pons y Moll, N.; Banse, F.; Miki, K.; Nierlich, M.; Girerd, J.-J. *Eur. J. Inorg. Chem.* **2002**, 1941−1944.

(92) Brinksma, J.; Rispens, M. T.; Hage, R.; Feringa, B. L. *Inorg. Chim. Acta* **2002**, *337*, 75−82.

reports similar differences with related ligands when switching from an ethyl to a propyl link.

Conclusion

Two new mononuclear Mn(II) complexes have been isolated and X-ray characterized, namely, *cis*-$[(L^2)Mn^{II}(Cl)_2]$ (**1**) and $[(L^3)Mn^{II}Cl(OH_2)](ClO_4)$ (**2**(ClO_4)). It is shown that, in the presence of 2,6-lutidine, after the total removal of the chloride ions, the exhaustive electrolysis leads to the formation of the mixed-valent di-μ-oxo-bridged dinuclear complexes $[(L)Mn^{III}(\mu\text{-}O)_2Mn^{IV}(L)](ClO_4)_3$ (respectively **3a**$(ClO_4)_3$ and **4**$(ClO_4)_3$).

Preparative-scale electrolyses were also performed on **1** and **2** in the absence of an external base. In the case of **1**, the mononuclear $[(L^2)Mn^{III}(Cl)_2]^+$ (**5**) complex is generated. In the case of **2**, the mono-μ-oxo-Mn(III)Mn(IV) mixed-valent species $[(L^3)ClMn^{III}(\mu\text{-}O)Mn^{IV}Cl(L^3)]^{3+}$ (**6**) is obtained as evidenced by its peculiar EPR signature. It is worth noting that thorough analysis of the EPR signatures is the key step allowing the differentiation between the di-μ-oxo and mono-μ-oxo bridges built in the mixed-valent complexes **4** and **6**. Species **6** is the third mono-μ-oxo-Mn_2(III,IV) compound in the literature for which the X-band EPR signature is fully described and simulated. This allows us to propose that isotropic Mn(III) hyperfine values slightly smaller than 130×10^{-4} cm^{-1} are a common and representative feature for such mixed-valent mono-μ-oxo-Mn_2(III,IV) species.

From the observed partial decoordination of the L^3 ligand and the role of the 2,6-lutidine in the building of the $[Mn(\mu\text{-}O)_2Mn]^{n+}$ core complexes, formation of the mono-μ-oxo-bridged species **6** would be assisted by the ligand itself as a base. It is remarkable that the substitution of the ethylene link in L^2 by a propylene link in the L^3 ligand results in such a drastically different solution behavior.

Acknowledgment. We are grateful to Félix Perez for mass spectrometry measurements and to Guillaume Blain for EPR technical assistance. We thank Dr. Alain Boussac (Service de Bioénergétique, URA CNRS 2096, CEA Saclay, Gif-sur-Yvette, France) for use of the EPR facilities and Pr. Jean-Jacques Girerd for stimulating discussions. The Conseil Régional de l'Ile de France for its contribution to the acquisition of the Bruker ELEXSYS 500 X-band EPR spectrometer and the COST D21 European action and the LRC-CEA project are acknowledged for their financial support.

Supporting Information Available: Figures showing the variation of the cyclic voltammograms of **2** upon addition of $AgClO_4$, experimental and simulated X-band EPR spectra of **3** and **4**, evolution of the X-band EPR spectrum of **2** during bulk electrolysis, UV−vis spectra of **4** and **6**, and cyclic voltammograms of **1** and **2** and tables listing the references of the published X-ray structures of mononuclear Mn(II) complexes with N_4Cl_2 and $M_4Cl(OH_2)$ coordination spheres and dinuclear $[N_4Mn^{III}\text{-}(\mu\text{-}O)_2\text{-}Mn^{IV}N_4]^{3+}$ (PDF). This material is available free of charge via the Internet at http://pubs.acs.org.

IC050243Y